Enzymological characterization of ^{64}Cu-labeled neprilysin substrates and their application for modulating the renal clearance of targeted radiopharmaceuticals

Brandt, F.; Ullrich, M.; Wodtke, J.; Kopka, K.; Bachmann, M.; Löser, R.; Pietzsch, J.; Pietzsch, H.-J.; Wodtke, R.;

Originally published:

January 2023

Journal of Medicinal Chemistry 66(2023)1, 516-537

DOI: https://doi.org/10.1021/acs.jmedchem.2c01472

Enzymological characterization of ^{64}Cu-labeled neprilysin substrates and their application for modulating the renal clearance of targeted radiopharmaceuticals

Florian Brandt[a,b], Martin Ullrich[a], Johanna Wodtke[a], Klaus Kopka[a,b,c,d], Michael Bachmann[a,c], Reik Löser[a,b], Jens Pietzsch[a,b], Hans-Jürgen Pietzsch[a,b], Robert Wodtke[a,*]

[a] Helmholtz-Zentrum Dresden-Rossendorf, Institute of Radiopharmaceutical Cancer Research, Bautzner Landstraße 400, 01328 Dresden, Germany

[b] Technische Universität Dresden, School of Science, Faculty of Chemistry and Food Chemistry, Mommsenstraße 4, 01069 Dresden, Germany

[c] National Center for Tumor Diseases (NCT) Dresden, University Hospital Carl Gustav Carus, Fetscherstraße 74, Dresden 01307, Germany

[d] German Cancer Consortium (DKTK), Partner Site Dresden, Fetscherstraße 74, 01307 Dresden, Germany

*E-mail: r.wodtke@hzdr.de

Abstract:

The applicability of radioligands for targeted endoradionuclide therapy is limited due to radiation-induced deleterious effects to healthy tissues. This applies in particular to the kidneys as primary organs of elimination, which requires dosimetric estimates to justify internal radionuclide therapy. In this context, the targeting of enzymes of the renal brush border membrane by cleavable linkers between target molecule and radiolabel that permit the formation of fast eliminating radionuclide-carrying cleavage fragments gains increasing interest. Herein, we synthesized a small library of ^{64}Cu-labeled cleavable linkers and quantified their substrate potentials toward neprilysin (NEP), a highly abundant peptidase at the renal brush border membrane. This allowed for the derivation of structure-activity relationships and selected cleavable linkers were attached to the somatostatin receptor subtype 2 ligand [Tyr^3]octreotate. Subsequent radiopharmacological characterization revealed that a substrate-based targeting of NEP in the kidneys with small molecules or peptides entails a certain degree of premature cleavage in the blood circulation by soluble and endothelium-derived NEP. However, for a tissue-specific targeting of NEP in the kidneys, the additional targeting of albumin in the blood by albumin-binding moieties is highlighted.

Introduction

Targeted endoradionuclide therapies, e.g. peptide receptor radionuclide therapy (PRRT), represent valuable approaches for the treatment of tumors and can lead to an unparalleled therapeutic success. They are based on radionuclide-labeled vector molecules/pharmacophores that address tumor-associated targets and by this action deliver the DNA-damaging radiation to the tumor cells.[1-3] A broad range of vector molecules ranging from low-molecular weight compounds to peptides and proteins were used for this purpose with peptide-based and peptidomimetic vectors attracting currently the highest interest. In this context, the most striking examples are certainly [^{177}Lu]Lu-DOTA-TATE[4] for targeting somatostatin receptor sub-type 2 (SST_2)-positive tumors and [^{177}Lu]Lu-PSMA-617[5] for targeting prostate-specific membrane antigen (PSMA)-positive tumors, which were recently approved as Lutathera® and Pluvicto™, respectively. The success of these radiopharmaceuticals stimulates the sustained search for novel targeted radiopharmaceuticals.[6, 7]

In general, the suitability of hydrophilic peptides or small molecules as vector molecules for PRRT or RLT can be attributed amongst others to their favorable pharmacokinetic properties, *i.e.* a fast tumor binding and a fast elimination from the body via the kidneys as primary excretion route.[8, 9] However, due to the often-observed prolonged retention of the intact radioligand or metabolites thereof in the kidneys, the absorbed dose in these organs usually limits the applicable activity amount (“dose”) of the radiopharmaceutical, which in turn affects the therapeutic window. Moreover, radiation-induced nephrotoxicity can occur as a severe side effect.[10, 11] The reason for a distinct kidney retention of a specific molecule is often not fully understood and might be various. For radiolabeled peptides and small proteins, a prominent mechanism is receptor-mediated endocytosis, which occurs after the glomerular filtration within the proximal tubule as part of the regular reabsorption process of nutrients. In this context, Marion de Jong and colleagues [12, 13] demonstrated that megalin, a type III transmembrane protein of 600 kDa which is localized in the plasma membrane on epithelial cells including proximal tubule cells (apical surface, microvilli),[14-16] significantly contributes to the observed kidney retention of radiolabeled somatostatin analogs, such as [^{111}In]In-DTPA-Octreotide and [^{177}Lu]Lu-DOTA-TATE. This was concluded amongst others from comparing the kidney uptake in mice with normal and without renal expression of megalin. Later, it was shown that also other radiolabeled peptides, including exendin, neurotensin and minigastrin, underly a megalin-dependent reabsorption, even though to a varying extent.[17] Once the receptor-radioligand complex is internalized, subsequent lysosomal degradation of the

radioligand leads to the formation of radiolabeled metabolites that can persist inside the proximal tubular cells. In case of [^{111}In]In-DTPA-Octreotide, [^{111}In]In-DTPA-D-Phe-Cys-OH and [^{111}In]In-DTPA-D-Phe-OH were identified as major metabolites and both compounds exhibit a long retention in the lysosomal compartment.[18, 19]

For lowering the kidney uptake of targeted radiopharmaceuticals, different strategies are pursued.[10, 11, 20, 21] The most successful approach so far and the standard procedure for the application of [^{177}Lu]Lu-DOTA-TATE is co-infusion of an amino acid solution consisting of the basic amino acids L-lysine and L-arginine (18-24 g of each in 1.5-2.2 L),[22] which is based on the early finding of Mogensen and Sølling regarding the inhibition of renal tubular protein reabsorption by certain amino acids.[23] Although this approach works well for somatostatin analogs and reduces the radiation dose to the kidneys between 35-59%,[22] it is accompanied by side-effects such as emesis or hyperkalemia and it is not necessarily effective for other radiopharmaceuticals.[20, 24] A more general strategy for lowering the radiation exposure of the kidneys is the structural modification of the radiopharmaceutical with a cleavable linker separating the vector molecule and the radiolabel, *i.e.* the radiometal-chelate complex. The linker is intended to be cleaved by enzymes of the renal brush border membrane and ideally, the formed small radiolabeled fragment is rapidly eliminated into the urine.[25, 26]

Pioneering work in the field of cleavable linkers for brush border membrane enzymes was performed by Yasushi Arano and colleagues based on their finding that a 3′-[^{131}I]iodohippuryl *N*$^{\varepsilon}$-maleoyl-lysine ([^{131}I]HML)-labeled antibody fragment (Fab) liberates [^{131}I]iodohippuric acid as the major radiometabolite into the urine leading to markedly reduced activity levels in the kidneys compared to directly labeled ^{125}I-Fab (via tyrosine residues).[27] Based on the analysis of the subcellular distribution of activity in the kidney, the authors concluded that [^{131}I]iodohippuric acid was most likely released already at the brush border membrane and not during lysosomal degradation. In contrast to the kidney uptake, the tumor uptake was not affected by the cleavable linker, which indicates that no significant premature release of [^{131}I]iodohippuric acid occurred in the blood circulation. The same group established an *in vitro* cleavage assay with brush border membrane vesicles (BBMVs) as source for renal brush border enzymes and demonstrated the enzyme-catalyzed release of [^{125}I]iodohippuric acid from model compounds such as 3′-[^{125}I]iodohippuryl L-lysine and 3′-[^{125}I]iodohippuryl *N*$^{\varepsilon}$-Boc-L-lysine.[28] Later, based on the glycine-lysine (GK) cleavage motif, the concept of cleavable linkers for targeting of renal brush border enzymes was also adapted to radiometal-labeled Fabs and GFK and MVK emerged as suitable cleavage sequences for the targeting of a distinct enzyme of the renal brush border membrane: neprilysin (neutral endopeptidase, NEP, CD10).[29-31]

NEP is a zinc-dependent membrane-bound metallopeptidase, which belongs to the M13 family (neprilysin family). Furthermore, it is a gluzincin due to its HEXXH zinc binding motif within the active site (histidine residues bind to Zn^{2+}) and a further glutamate residue aside from this motif acting as third Zn^{2+} ligand.[32] It cleaves a broad range of biologically active peptides including enkephalins, atrial natriuretic peptides (ANP), endothelins, bradykinin, and somatostatin, which highlights the important role of NEP as a regulatory enzyme. Moreover, its involvement in different pathophysiological situations such as heart failure, Alzheimer's disease and different kinds of cancer renders NEP an attracting diagnostic biomarker and therapeutic target.[33-36] It is widely expressed in mammals, but it is of particular abundance in the intestinal and renal brush border membrane (microvilli), with the latter representing the tissue where the enzyme was firstly discovered.[37, 38] The high abundance of NEP within the renal brush border membrane renders this enzyme an apparently ideal target for the design of cleavable linkers.

Although recent studies were focused on optimizing the linker sequences toward an enhanced enzymatic cleavage rate,[39, 40] no quantitative data on the distinct substrate potential toward NEP or other brush border membrane enzymes are reported, which would lay the basis for a rationalized use of this strategy. Furthermore, the concept of cleavable linkers was predominantly applied to antibody derivatives and large peptides, such as exendin-4,[39, 41, 42] but only few studies are reported on adapting this strategy to small molecules or peptides.[43, 44] Herein, we synthesized a series of ^{64}Cu-labeled tri- and tetrapeptides and quantified their suitability to act as **ne**prilysin **s**ubstrates (NES) in a radiometric assay using recombinant NEP, which led to the exploration of the structural features that drive the cleavage rate. The specificity for cleavage by NEP was assessed *in vitro* in human plasma by the use of specific inhibitors. Subsequently, selected peptides were chosen for modifying the known somatostatin analog [Tyr^3]octreotate (TATE) with the aim of studying the kidney uptake in dependence on the cleavage rate by NEP. The substrate potential and specificity of the resulting **[^{64}Cu]Cu-NODAGA-NES-TATEs** were again assessed *in vitro* in both human and mouse plasma. For further radiopharmacological characterization *in vitro* and *in vivo*, an in-house mouse pheochromocytoma (MPC) tumor allograft model with high levels of SST_2 was used.[45-47] Accordingly, the present study is part of our current efforts on modulating the pharmacokinetic properties of radioligands by systematic structural modifications and adds to our previous work on TATE derivatives bearing albumin binders.[47]

Results and Discussion

*Design and synthesis of neprilysin substrates (compounds **1**-**6**)*

The widely used strategy for the introduction of cleavable linkers relies on labeling the vector molecule at cysteine residues by the use of a maleimide-functionalized lysine within the GFK and MVK sequences. As chelator for subsequent labeling with the desired radiometal, NOTA-Bn-NCS is often incorporated via a thiourea functionality at the N-terminus of the peptides. This structural motif set the basis for the design of the neprilysin substrates herein, but instead of maleimide-based conjugation, we envisaged “clickable” peptides by substituting lysine by ε-azido-norleucine, which accounts for stereochemically homogenous constructs. The synthesis of the peptides (Scheme S1 in Supporting Information) was performed with polymeric support starting from anchoring of Fmoc-Lys(N_3)-OH onto the 2-ClTrt-Cl or Rink-amide resins. Common conditions for amino acid coupling (HATU/DIPEA), Fmoc removal (20% piperidine in DMF) and cleavage from the resin (TFA) were used. Overall, eleven peptides were synthesized and obtained in moderate to good overall yields (9-33%) after purification by RP-HPLC. The peptides can be classified into 6 groups based on their differences in the amino acid sequence, the chelator moiety and the C-terminal modification (Figure 1).

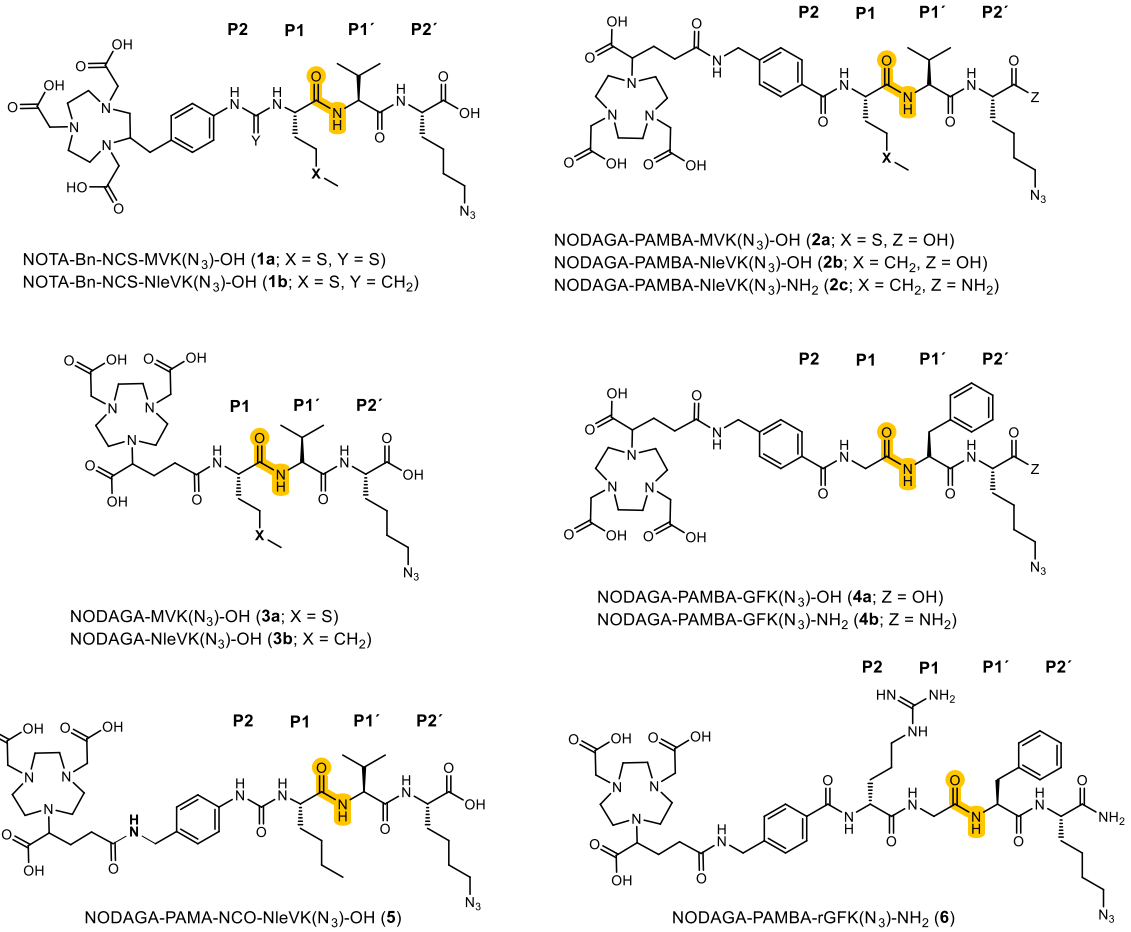

Figure 1. Structures of the tri- and tetrapeptide-derived NEP substrates

The amino acid residues around the cleavage site for NEP were labeled according to the Schechter and Berger[48] nomenclature.

Table 1. Analytical data of the synthesized NEP substrates

compound	Chemical formula	m/z calculated for $[M+H]^+$	m/z found for $[M+H]^+$ [a]	Purity (%)[b]
1a	$C_{36}H_{56}N_{10}O_{10}S_2$	853.3695	853.3697	≥95
1b	$C_{37}H_{58}N_{10}O_{10}S$	835.4131	835.4131	≥96
2a	$C_{39}H_{60}N_{10}O_{12}S$	893.4186	893.4190	≥98
2b	$C_{40}H_{62}N_{10}O_{12}$	875.4621	875.4623	≥99
2c	$C_{40}H_{63}N_{11}O_{11}$	874.4781	874.4788	≥99
3a	$C_{31}H_{53}N_9O_{11}S$	760.3658	760.3657	≥98
3b	$C_{32}H_{55}N_9O_{11}$	742.4094	742.4101	≥99
4a	$C_{40}H_{54}N_{10}O_{12}$	867.3995	867.3998	≥99
4b	$C_{40}H_{55}N_{11}O_{11}$	866.4155	866.4159	≥98
5	$C_{40}H_{63}N_{11}O_{12}$	890.4736	890.4728	≥99
6	$C_{46}H_{67}N_{15}O_{12}$	1022.5166	1022.5167	≥97
		m/z calculated for $[M+2H]^{2+}$	**m/z found for $[M+2H]^{2+}$ [a]**	
NODAGA-NES1-TATE	$C_{87}H_{128}N_{20}O_{25}S_2$	959.4479	959.4483	≥99
NODAGA-NES2-TATE	$C_{95}H_{135}N_{21}O_{26}S_2$	1025.9737	1025.9751	≥97
NODAGA-NES3-TATE	$C_{95}H_{127}N_{21}O_{26}S_2$	1021.9424	1021.9433	≥98
NODAGA-NES4-TATE	$C_{101}H_{139}N_{25}O_{27}S_2$	1099.9930	1099.9937	≥96
NODAGA-NES5-TATE	$C_{122}H_{166}IN_{27}O_{31}S_2$	1349.0438	1349.0435	≥98

[a]High-resolution mass spectra using electrospray ionization were recorded. [b]Purity was determined by analytical RP-HPLC and is given for 230 nm.

*Radiolabeling and kinetic characterization of ^{64}Cu-labeled compounds **1**-**6***

For the kinetic characterization of peptides **1**-**6** toward recombinant NEP, a radiometric assay was envisaged, in which the formation of cleavage products and the disintegration of the intact compound is followed by analytical radio-HPLC. To this end, the peptides were labeled with $[^{64}Cu]CuCl_2$, incubated with enzyme in PBS buffer (pH 7.4, 37°C) and aliquots were withdrawn at distinct time points (0.5, 1, 2, 4, and 24 h, see Figure 2). In this context, the non-metalated peptides were not removed after radiolabeling and the total concentration of both species for the radiometric assay was adjusted around 7 µM based on the apparent molar activity. This required the addition of 10 µM $ZnCl_2$ (resulting in approx. 3 µM free Zn^{2+}) to the reaction mixtures as the concentration of the enzyme (15 nM) was far below that of the peptides. Otherwise, Zn^{2+} within the active center of NEP would be complexed by any present NOTA or NODAGA. The alternative of adding $CuCl_2$ to saturate any non-labeled chelator was not followed due to the known inhibitory activity of Cu^{2+} toward NEP (K_i of 1.04 µM). Worth of note, also Zn^{2+} exerts an inhibitory activity, but this becomes relevant at significantly higher concentrations (K_i of 19.5 µM) compared to Cu^{2+}.[49]

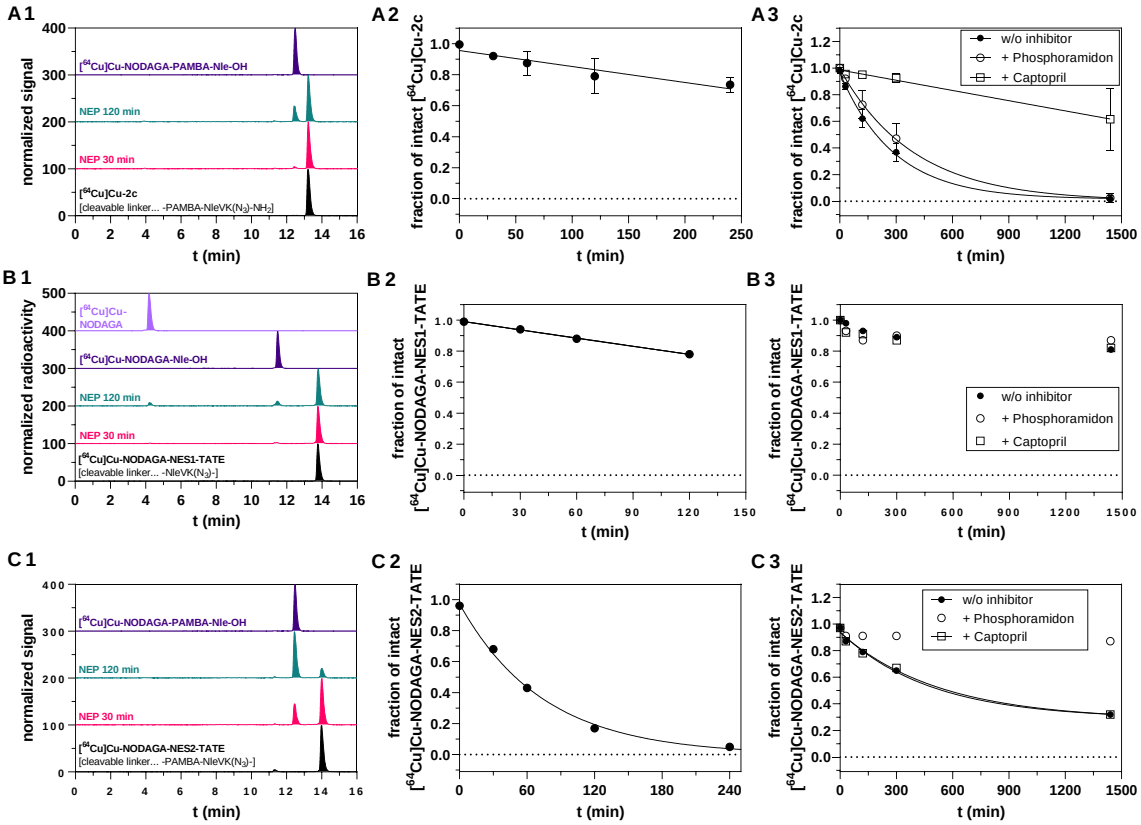

Figure 2. Time-dependent cleavage of the ^{64}Cu-labeled peptides 2c (A), NODAGA-NES1-TATE (B) and NODAGA-NES2-TATE (C) toward NEP and in human plasma

A1/B1/C1) Exemplary HPLC chromatograms of **[^{64}Cu]Cu-2c** (black, t_R=13.4 min), **[^{64}Cu]Cu-NODAGA-NES1-TATE** (black, t_R=13.8 min) and **[^{64}Cu]Cu-NODAGA-NES2-TATE** (black, t_R=14.0 min), after subsequent incubation with NEP for 30 min (pink) and 120 min (green) and of the respective cleavage fragments **[^{64}Cu]Cu-NODAGA-PAMBA-Nle-OH** (purple, t_R=12.6 min), **[^{64}Cu]Cu-NODAGA-Nle-OH** (purple, t_R=11.5 min) and **[^{64}Cu]Cu-NODAGA** (light purple, t_R=4.2 min). **A2/B2/C2**) Plots of residual intact radiolabeled peptide *versus* time for the NEP incubations with nonlinear regression according to one-phase decay. **A3/B3/C3**) Plots of residual intact radiolabeled peptide after incubation in human plasma under different conditions with nonlinear regression according to one-phase decay. NEP and plasma incubations were performed at 37 °C for 24 h and aliquots were withdrawn at distinct time points for examining the disappearance of the radiolabeled peptide. Concentration of phosphoramidon and captopril was adjusted to 10 µM. Data shown are mean values (±SD) of 1 (**B2**, **B3**, **C2**, **C3**), 2 (**A2**) and 2-4 (**A3**) single experiments.

A time-dependent disintegration accompanied by the formation of one distinct radiolabeled cleavage fragment was observed for most of the compounds. The retention times of the cleavage fragments (Figure 3 and Table 2) are in accordance with that of the anticipated compounds, which were separately synthesized, radiolabeled and analyzed using the same HPLC conditions (Figure S1 in Supporting Information). Plotting the fraction of intact ^{64}Cu-labeled peptide *versus* time provided curves with a linear or exponential decline (Figure 2 and Figure S1 in Supporting Information). Analysis was done by linear and non-linear regression according to one-phase decay, respectively, to obtain the values for the rate constant k_{obs}. This first order rate constant (in s^{-1}) can be transformed into the pseudo second order rate constant

k_{obs}/[E] (in $M^{-1}s^{-1}$) as a measure of the substrate potential. The rationale for this can be given considering the Michaelis-Menten equation (I)

$$v = \frac{V_{max} * [S]}{[S]+K_m} \quad \text{(I)}$$

or the similar expression (II), where V_{max} is substituted with the product of k_{cat} and [E].

$$v = \frac{k_{cat}*[E] * [S]}{[S]+K_m} \quad \text{(II)}$$

Generally, the Michaelis-Menten relation applies only for substrate conversions where the enzyme concentration is far below that of the substrate ([E]<<[S]). As the fraction of intact peptide was plotted *versus* time, equation II can be transformed to equation III by substituting the quotient v/[S] by k_{obs}.

$$k_{obs} = \frac{k_{cat}*[E]}{[S]+K_m} \quad \text{(III)}$$

Dividing k_{obs} by [E] yields the following relation.

$$\frac{k_{obs}}{[E]} = \frac{k_{cat}}{[S]+K_m} \quad \text{(IV)}$$

For the case [S]<<K_m, equation IV could be further simplified to equation V and k_{obs}/[E] would be equal to the performance constant k_{cat}/K_m, a common measure of the substrate potential.

$$\frac{k_{obs}}{[E]} = \frac{k_{cat}}{K_m} \quad \text{(V)}$$

However, the K_m values of the peptides are not known and considering the applied concentration of around 7 µM for the radiolabeled compounds **1**-**6** and reported K_m values of similar peptides such as the FRET substrates Abz-RGFK(Dnp)-OH (K_m of 14 µM) and Abz-RGFK(Dnp)-NH_2 (K_m of 25.9 µM),[50] it appears unlikely that [S]<<K_m is given in the present radiometric assay. Therefore, the different radiolabeled peptides were compared based on the k_{obs}/[E] values.

^{64}Cu-labeling (20 min at 60°C) of NOTA-Bn-NCS-MVK(N_3) (**1a**) proceeded almost quantitatively regarding residual free [^{64}Cu]$CuCl_2$, however, several radiolabeled species were obtained in addition to [^{64}Cu]Cu-**1a** resulting in an only fair radiochemical purity of 72% (Supporting Information). No improvement has been achieved by using mild labeling conditions (10 min at room temperature). Similarly, ^{64}Cu-labeling of the Nle analog of **1a**, compound **1b**, resulted in an insufficient radiochemical purity of 57% (Supporting Information). The thiourea functionality at the N-terminus in both compounds might be causative for the observed results

considering the phenomena of thione-thiol tautomerization[51, 52] and potential Edman degradation.[53-55] Moreover, the occurrence of different isomers of ^{64}Cu-labeled NOTA-Bn-amine is known.[56] In this context, similar radioactivity-detected HPLC chromatograms for [^{64}Cu]Cu-NOTA-Bn-NCS functionalized peptides were occasionally observed.[57] Worth of note, the HPLC analyses of the non-labeled peptides **1a** and **1b** prior to radiolabeling revealed good purities (95 and 96% respectively, Table 1). Despite the unfavorable radiochemical purity of **[^{64}Cu]Cu-1a**, incubations with NEP were performed. A slow cleavage to **[^{64}Cu]Cu-NOTA-Bn-NCS-M-OH** (Figure 3, Table 2) could only be detected at an elevated enzyme concentration of 69 nM (instead of 15 nM) with >50% of **[^{64}Cu]Cu-1a** being cleaved after 24 h, however, quantification by means of k_{obs}/[E] was hampered due to crowded radioactivity-detected HPLC traces (Figure S1 in Supporting Information).

Facing the radiochemical challenges with NOTA-Bn-NCS, we decided to change the N-terminal group to NODAGA-PAMBA, which closely resembles the original structure but is attached via an amide bond instead of a thiourea functionality. A similar approach was recently followed by Bendre *et al.*[44] for the introduction of cleavable linkers into PSMA ligands. As expected, ^{64}Cu-labeling of **2a** yielded a higher radiochemical purity (≥94%) compared to labeling of **1a** and **1b**. Moreover, a time-dependent cleavage upon incubation with NEP (15 nM) was observed with a quantitative cleavage to **[^{64}Cu]Cu-NODAGA-PAMBA-M-OH** being reached after 4 h. Based on the aforementioned mathematical derivation, a k_{obs}/[E] value of 25,800 $M^{-1}s^{-1}$ has been calculated. Replacement of methionine by norleucine as realized in **[^{64}Cu]Cu-2b** resulted in a similar substrate potential with a k_{obs}/[E] of 17,600 $M^{-1}s^{-1}$. This is of particular importance as methionine is prone to oxidation to the respective methionine sulfoxide under acidic conditions applied for solid-phase peptide synthesis, which is not recognized by NEP.[44] In this context, another bioisosteric substitution would be methoxinine,[58] which however, was not tested herein. The formal C-terminal amidation of **[^{64}Cu]Cu-2b** led to **[^{64}Cu]Cu-2c**, which is still recognized by NEP but the substrate potential is markedly decreased (k_{obs}/[E] of 1,100 $M^{-1}s^{-1}$, factor of 16, see Figure 2 A1). This result is in accordance to previous data showing that the carboxydipeptidase activity of NEP is higher than its endopeptidase activity.[50] In another set of compounds, the influence of the N-terminal benzoyl group, *i.e.* the PAMBA group, on the substrate potential was investigated. The removal of this group decreased the substrate potential to a similar extent as C-terminal amidation as seen on the basis of the k_{obs}/[E] values of 610 and 1,100 $M^{-1}s^{-1}$ for compounds **[^{64}Cu]Cu-3a** and **[^{64}Cu]Cu-3b**, respectively, in comparison to the k_{obs}/[E] value of **[^{64}Cu]Cu-2b** (17,600 $M^{-1}s^{-1}$).

In addition to MVK, GFK was described as suitable cleavage sequence for NEP. Both sequences exhibit a bulky hydrophobic amino acid in P1' (V and F), which is preferred by

NEP.[36] Therefore, **NODAGA-PAMBA-GFK(N_3)-OH** (**4a**) and its C-terminally amidated analog **4b** were synthesized. **[^{64}Cu]Cu-4a** exhibits a 6-times higher substrate potential (k_{obs}/[E] of 107,000 $M^{-1}s^{-1}$) than the corresponding NleVK(N_3) analog **[^{64}Cu]Cu-2b**. Again, C-terminal amidation reduced the substrate potential to a similar extent (k_{obs}/[E] of 12,600 $M^{-1}s^{-1}$, factor of 8) as seen for the NleVK pair **2a** and **2b**.

The fundamental difference in the cleavage rate of compounds **[^{64}Cu]Cu-1a** and **[^{64}Cu]Cu-2a**/**2b** indicates that the thiourea functionality is detrimental for the recognition by NEP. To this end, **NODAGA-PAMA-NCO-NleVK(N_3)-OH** (**5**) was synthesized, in which the PAMBA moiety of **2a**/**2b** is substituted by *p*-aminomethylaniline (PAMA), which is coupled via a urea functionality at the N-terminus of the NleVK peptide. Similar to [^{64}Cu]Cu-**1a**, cleavage of **[^{64}Cu]Cu-5** to the expected fragment **NODAGA-PAMA-NCO-Nle-OH** (Figure 3, Table 2) could only be detected at an elevated NEP concentration of 69 nM. The high radiochemical purity of **[^{64}Cu]Cu-5** enabled the derivation of the k_{obs}/[E] value to 70 $M^{-1}s^{-1}$ (8% cleavage fragment after 4 h). Therefore, the formal substitution of the N-terminal amide bond in **[^{64}Cu]Cu-2b** (k_{obs}/[E] of 17,600 $M^{-1}s^{-1}$) by an urea functionality resulted in a 250-fold reduction of the apparent substrate potential proving the hypothesis that a N-terminal (thio)urea functionality is detrimental for the recognition by NEP. A potential explanation for this might be the fact that the conformational flexibility of the NODAGA-PAMA-carbamoyl residue in **[^{64}Cu]Cu-5** is lowered due to the additional barrier for the rotation of the N-CO bond adjacent to the phenyl ring. Consequently, a favorable alignment within the active site of NEP might be hindered. Uehara *et al.*[30] reported that **[^{67}Ga]Ga-NOTA-Bn-NCS-MVK(Benzoyl)-OH** released up to 19% of **[^{67}Ga]Ga-NOTA-Bn-NCS-M-OH** upon incubation with BBMVs over 2 h (NEP concentration is unknown). Furthermore, Suzuki *et al.*[59] recently characterized **[^{64}Cu]Cu-NOTA-Bn-NCS-M-OH** toward cleavage using BBMVs and noted a significantly slower cleavage compared to the ^{67}Ga-labeled analog. Therefore, the really slow cleavage rate of the ^{64}Cu-labeled (thio)urea compounds herein appears in line with these previous reports.

For the last compound within this small library of peptides, **NODAGA-PAMBA-rGFK(N_3)-NH_2** (**6**), the central tripeptide was extended to an tetrapeptide (rGFK), as D-Arg in Position P2 is known to increase the cleavage rate by NEP and also the specificity of the cleavage, in particular toward ACE and trypsin.[50, 60] A k_{obs}/[E] value of 52,500 $M^{-1}s^{-1}$ has been determined for **[^{64}Cu]Cu-6**, which highlights the favorable effect of D-Arg in P2 as the substrate potential is 4-times higher than that of the corresponding GFK analog **[^{64}Cu]Cu-4b**.

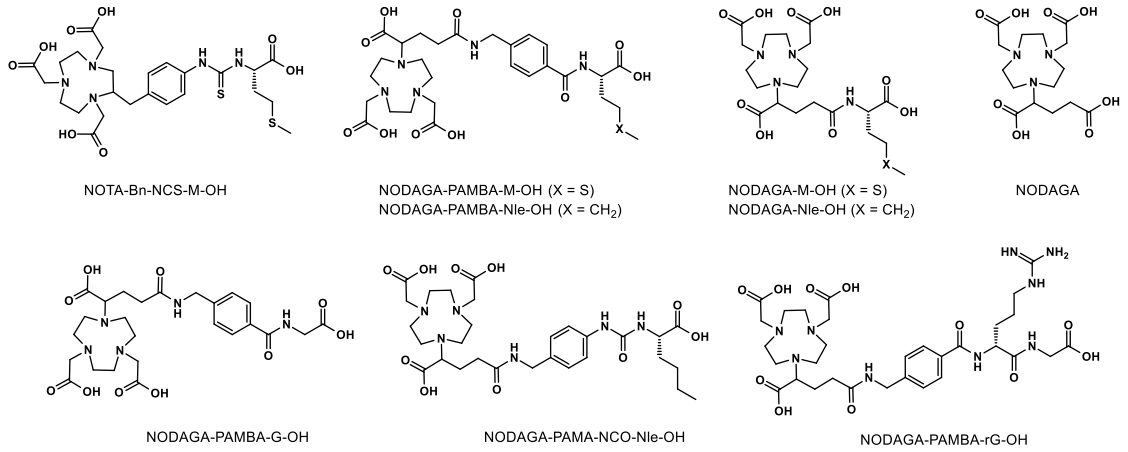

Figure 3. Structures of cleavage fragments

Table 2. Assignment of cleavage fragments to their parent peptides

compound	**fragment of**
NOTA-Bn-NCS-M-OH	**1a**
NODAGA-PAMBA-M-OH	**2a**
NODAGA-PAMBA-Nle-OH	**2b, 2c, NODAGA-NES2-TATE**
NODAGA-M-OH	**3a**
NODAGA-Nle-OH	**3b, NODAGA-NES1-TATE**
NODAGA	**NODAGA-NES1-TATE**
NODAGA-PAMBA-G-OH	**4a, 4b, NODAGA-NES3-TATE**
NODAGA-PAMA-NCO-Nle-OH	**5**
NODAGA-PAMBA-rG-OH	**NODAGA-NES4-TATE, NODAGA-NES5-TATE**

Table 3. Summary of *in vitro* cleavage data for the ^{64}Cu-labeled NEP substrates

^{64}Cu-labeled cpd. (cleavage sequence)	k_{obs}/[E] ($M^{-1}s^{-1}$)[a]		$t_{1/2,\ hum.\ pl.}$ (min)[a]		$t_{1/2,\ m.\ pl.}$ (min)[a]		ACE[b]
	mean	CI of 68%	mean	CI of 68%	mean	CI of 68%	
1a (-Bn-NCS-MVK(N_3)-OH)	*n.q.*[c]		>1440		*n.d.*		-
2a (-PAMBA-MVK(N_3)-OH)	25,800	24,800-26,700	<10		*n.d.*		*n.d.*
2b (-PAMBA-NleVK(N_3)-OH)	17,600	15,400-20,000	13	11-14	*n.d.*		+
2c (-PAMBA-NleVK(N_3)-NH_2)	1,100	900-1,100	199	184-216	*n.d.*		+
3a (-MVK(N_3)-OH)	610	460-760	*n.d.*		*n.d.*		*n.d.*
3b (-NleVK(N_3)-OH)	1,100	700-1,400	9	8-10	*n.d.*		+
4a (-PAMBA-GFK(N_3)-OH)	107,000	105,000-109,000	35	32-38	*n.d.*		+
4b (-PAMBA-GFK(N_3)-NH_2)	12,600	8,800-18,100	193	177-211	*n.d.*		+
5 (-PAMA-NCO-NleVK(N_3)-OH)	70	64-83	*n.d.*		*n.d.*		*n.d.*
6 (-PAMBA-rGFK(N_3)-NH_2)	52,500	44,900-49,800	95	90-101	*n.d.*		-
NES1 (-NleVK(N_3)-)	1,950	1,880-2,010	>1,440		540	430-730	-
NES2 (-PAMBA-NleVK(N_3)-)	14,800	13,600-16,100	340	260-470	390	310-530	-
NES3 (-PAMBA-GFK(N_3)-)	48,700	29,100-97,200	350	320-390	>1,440		-
NES4 (-PAMBA-rGFK(N_3)-)	109,000	84,700-216,000	91	88-95	450	250-1,930	-
NES5 (-PAMBA-rGFK(cLAB)-)	42,800	35,300-52,800	>1,440		>1,440		-

For a better overview, the N-terminal chelator moiety (NOTA for **1a** and NODAGA for all other compounds) was omitted. The structures of the compounds are depicted in Figure 1 and Figure 5. [a]Data shown for k_{obs}/[E] and plasma half-lives are derived from 1-4 single experiments. For the NEP incubations, 15, 30 or 69 nM of NEP and ~7 µM of radiolabeled peptide were used. Values of k_{obs}/[E] and plasma half-lives were obtained from plots of residual intact radiolabeled peptide by linear regression or nonlinear regression according to one-phase decay (see experimental section). [b]Susceptibility of the peptides to ACE cleavage was assessed with plasma incubations in the presence of captopril (10 µM) and is qualitatively specified with "+" (peptide is a ACE substrate) and "-" (peptide is no ACE substrate). [c]n.q. denotes "not quantifiable", but >50% of **[^{64}Cu]1a** is cleaved after 24 h with 69 nM NEP. *n.d.* denotes "not determined".

*Assessing the cross-reactivity of the ^{64}Cu-labeled compounds **1**-**6** in human plasma*

Besides quantifying the substrate potential of the peptides, the specificity for the NEP-mediated cleavage is crucial to assess. Considering the *i.v.* application route for targeted radiopharmaceuticals, the stability in blood is of particular importance. Therefore, we envisaged the investigation of the stability of the ^{64}Cu-labeled peptides **1**-**6** in human plasma after different time points in the absence and in the presence of two inhibitors (Figure 2): phosphoramidon and captopril (Figure 4). Phosphoramidon is a potent inhibitor of NEP with reported IC_{50} values in the single to double-digit nM range (e.g. 80 nM at pH 7.4[61], herein determined to 27 nM using **[^{64}Cu]Cu-6**, Figure S2 in Supporting Information), while captopril is a potent inhibitor of another Zn^{2+}-dependent metalloprotease, angiotensin-converting enzyme (ACE, e.g. IC_{50} of 20 nM[62]). Cross-reactivity of the peptides in plasma can be anticipated, in particular for peptides with a free C-terminus, considering the known activity of both proteases toward the same biologically active peptides.[63] The concentration of both inhibitors had to be carefully chosen as too high concentrations might also markedly inhibit the other protease (e.g. IC_{50} of 78 µM for phosphoramidon toward ACE is reported).[64] Therefore, both inhibitors were applied in a concentration of 10 µM.

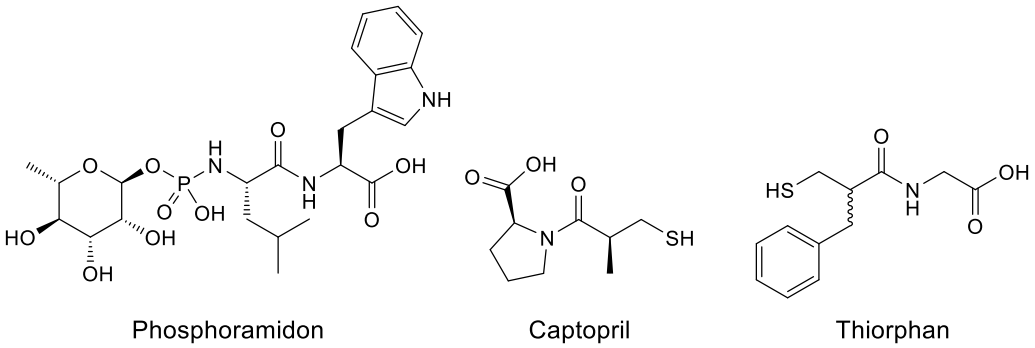

Figure 4. Structures of phosphoramidon, captopril and thiorphan

Incubating **[^{64}Cu]Cu-1a** in human plasma, even though the radiochemical purity was low, revealed no detectable degradation. In contrast, the peptides with an N-terminal amide group showed a time-dependent degradation, which allowed for the calculation of the respective half-lives (Table 3). Worth of note, the observed radiolabeled fragments are in accordance to the fragments observed for the incubations with recombinant NEP (Figure S1 in Supporting Information). The lowest plasma stability was observed for the ^{64}Cu-labeled peptides **2a**, **2b**, **3b**, and **4a** with plasma half-lives between 9 and 35 min. The common structural feature of these peptides is the free C-terminus and in accordance to that, incubation in human plasma in the presence of captopril raised the plasma half-life to >24 h (Figure S1 in Supporting Information), highlighting the pronounced substrate potential toward ACE. Incubation in the presence of phosphoramidon had no influence on the rate of degradation. C-terminal amidation positively influenced the stability in human plasma as seen for the half-lives of the ^{64}Cu-labeled peptides **2c** (Figure 2 A3) and **4b** (approx. 200 min, Table 3). However, both peptides are still substrates for ACE as the half-lives are increased to >24 h in the presence of captopril. Only a slight increase in the half-lives in the presence of phosphoramidon has been observed (Figure S1 in Supporting Information). The prevention of ACE-catalyzed cleavage was achieved by the introduction of D-Arg in P2 for **[^{64}Cu]Cu-6**, even though the half-life was not increased compared to **[^{64}Cu]Cu-4b** (193 and 95 min, respectively). The main reason might be that **[^{64}Cu]Cu-6** is a 4-times better substrate for NEP than **[^{64}Cu]Cu-4b** and the NEP-catalyzed cleavage is now the dominant enzymatic conversion of **[^{64}Cu]Cu-6** in human plasma. Accordingly, the incubation in the presence of phosphoramidon increased the half-life to almost 24 h.

(Radio)synthesis, kinetic characterization toward NEP and radiopharmacological in vitro characterization of the [^{64}Cu]Cu-NODAGA-NES(1-4)-TATEs

The kinetic characterization of the ^{64}Cu-labeled peptides **2**-**6** revealed substrate potentials toward NEP by means of k_{obs}/[E] over three order of magnitude (70-107,000 $M^{-1}s^{-1}$). For studying the targeting of renal NEP in dependence of the particular substrate potential and considering the improved specificity for NEP over ACE of C-terminally amidated peptides, we decided to attach selected **ne**prilysin **s**ubstrates (**NES**), based on peptides **2c**, **3b**, **4b**, and **6**, to the SST_2 agonist TATE at the N-terminus, separated by a mini PEG2 linker, rather than the introduction via click reaction. Of course, this makes the azide group superfluously, however, we kept this functionality for a potential additional structural modification (see **NODAGA-NES5-TATE** below). The resulting **NODAGA-NES(1-4)-TATEs** (Figure 5) were synthesized by solid-phase synthesis using an automated microwave peptide synthesizer (Biotage Initiator+ Alstra, Scheme S2 in Supporting Information). All peptides were obtained in overall yields ranging from 4 to 7% and in good chemical purities (≥96%, Table 1). ^{64}Cu-labeling was performed in orientation to the labeling of the peptides **1**-**6** and afforded the **[^{64}Cu]Cu-NODAGA-NES(1-4)-TATEs** in good radiochemical yields and purities (≥98%, see the Supporting Information for radioactivity-detected chromatograms).

The substrate potential of the **[^{64}Cu]Cu-NODAGA-NES(1-4)-TATEs** was assessed toward recombinant NEP as described above, which revealed k_{obs}/[E] values that increase in the order of numbering (1,950-109,000 $M^{-1}s^{-1}$). However, the absolute values are higher than anticipated based on the corresponding isolated small peptides (factors of 2-13) indicating that a secondary amide at the C-terminus is better tolerated by NEP than a primary amide. While for the **[^{64}Cu]Cu-NODAGA-NES(2-4)-TATEs**, the expected radiolabeled cleavage fragments were observed, incubation of **[^{64}Cu]Cu-NODAGA-NES1-TATE** with NEP resulted in the formation of a second radiolabeled cleavage fragment in addition to **[^{64}Cu]Cu-NODAGA-Nle-OH** (Figure 2 B). Based on the HPLC retention with the authentic compound, the second metabolite was identified as **[^{64}Cu]Cu-NODAGA**, which is formed at a similar rate as **[^{64}Cu]Cu-NODAGA-Nle-OH**. Worth of note, the NEP-catalyzed cleavage between NODAGA and Nle was not observed for **NODAGA-NIeVK(N_3)-OH** (**3b**), most likely because the carboxydipeptidase activity of NEP is dominant for this compound.

Incubating the **[^{64}Cu]Cu-NODAGA-NES(1-4)-TATEs** in human plasma in the presence of captopril revealed that they are not recognized by ACE anymore (Table 3, Figure 2 B/C and Figure 6). Therefore, the tolerance between primary and secondary amide appears contrary between NEP and ACE. The stability of the **[^{64}Cu]Cu-NODAGA-NES(1-4)-TATEs** in human

plasma is in accordance to their substrate potentials toward NEP and the degradation has been completely blocked in the presence of phosphoramidon.

Due to the intended radiopharmacological characterization in mice, the stability in mouse plasma was also of interest (Table 3, Figure 6, and Figure S1 in Supporting Information). Here, **[^{64}Cu]Cu-NODAGA-NES1-TATE** and **[^{64}Cu]Cu-NODAGA-NES2-TATE** exhibited neither an ACE nor a NEP dependent cleavage, which suggests the action of (a) further protease(s). However, both compounds are stilled transformed to the same radiolabeled metabolites as observed upon incubation with NEP. In contrast, NEP-catalyzed cleavage in mouse plasma has been detected for **[^{64}Cu]Cu-NODAGA-NES3-TATE** and **[^{64}Cu]Cu-NODAGA-NES4-TATE**, but the concentration of soluble NEP is obviously lower in mouse than in human plasma, which explains the significantly increased half-lives of both compounds (350 and 91 min in human plasma and >1,440 and 448 min in mouse plasma).

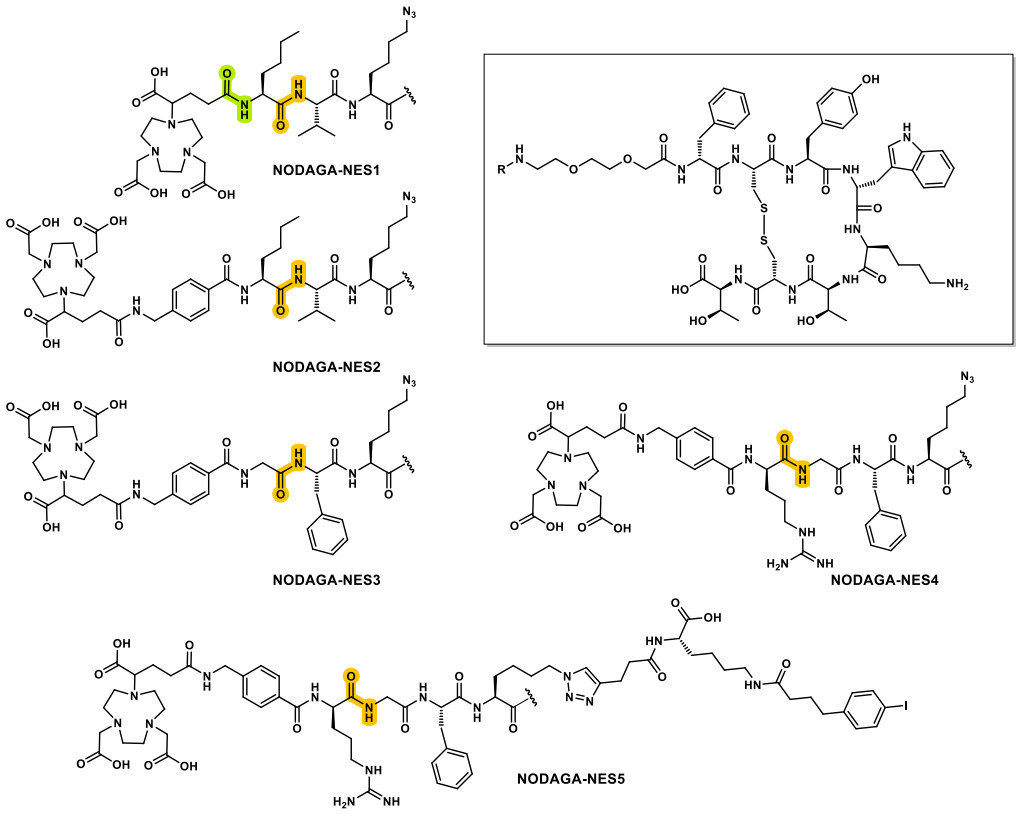

Figure 5. Structures of NODAGA-NES-TATEs used for radiopharmacological characterization *in vitro* and *in vivo*

The cleavage sites for NEP are highlighted in orange. For **NODAGA-NES1-TATE**, a second cleavage site was observed, which is highlighted in green. Amino acid sequence of TATE: D-Phe-c(Cys-Tyr-D-Trp-Lys-Thr-Cys)-Thr.

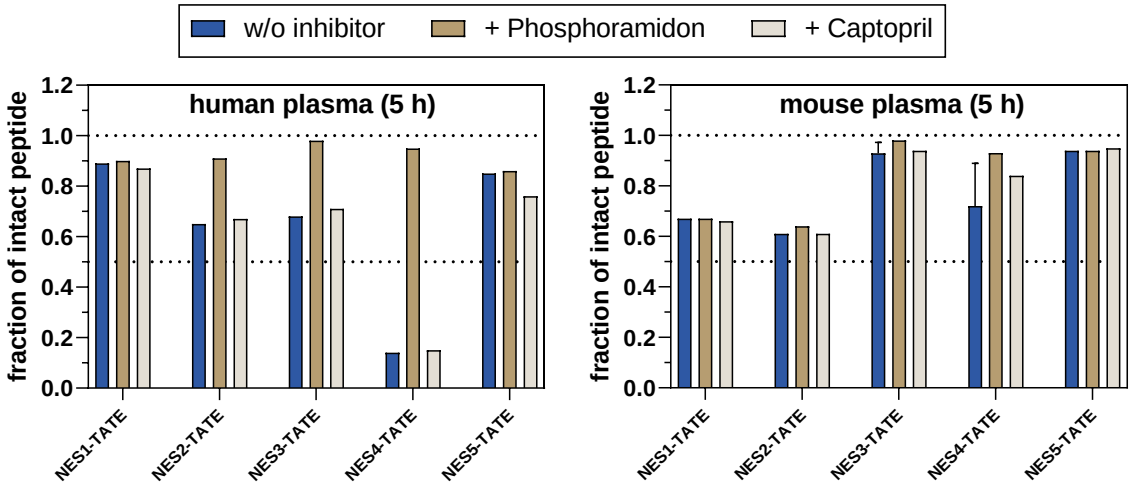

Figure 6. Stability of ^{64}Cu-labeled NODAGA-NES-TATEs in human and mouse plasma

Bar plots of residual intact radiolabeled peptide in human and mouse plasma after 5 h under different conditions. Concentration of phosphoramidon and captopril was adjusted to 10 µM. Data shown are derived from 1-2 single experiments for each radiolabeled peptide.

Table 4. Summary of log$D_{7.4}$ and SST_2 binding data for the ^{64}Cu-labeled TATE derivatives

compound	log$D_{7.4}$[a]	K_d[SST_2] (nM)[b]	B_{max} (fmol/mg of protein)[b]
[^{64}Cu]Cu-NODAGA-NES1-TATE	-2.54 (0.03)	2.36 (2.10-2.66)	303 (293-313)
[^{64}Cu]Cu-NODAGA-NES2-TATE	-2.13 (0.08)	2.09 (1.78-2.45)	256 (243-265)
[^{64}Cu]Cu-NODAGA-NES3-TATE	-2.60 (0.10)	2.76 (2.33-3.25)	371 (354-389)
[^{64}Cu]Cu-NODAGA-NES4-TATE	-2.45 (0.10)	2.65 (1.93-3.64)	586 (532-649)
[^{64}Cu]Cu-NODAGA-NES5-TATE	-2.20 (0.14)	3.73 (3.30-4.21)	583 (563-603)

[a]Data shown are mean values (±SD) of three separate processes of shaking out. [b]Data shown are mean values with calculated confidence interval of 68% of one experiment, which was performed in duplicate using live mouse pheochromocytoma (MPC) cells. For comparison, K_d and B_{max} values of 3.17 (2.81-3.57) nM and 649 (629-670) fmol/mg of protein, respectively, were obtained for **[^{64}Cu]Cu-NODAGA-TATE** under the same experimental conditions.

Prior to a radiopharmacological characterization *in vivo*, the SST_2 affinity was evaluated. In our previous study on ^{64}Cu-labeled TATE derivatives bearing albumin binders, a radioligand binding assay using mouse pheochromocytoma cell lysates was applied.[47] Herein, the assay was changed to live MPC cells, which proved to be more convenient than the use of cell lysates due to the occasionally observed high non-specific binding of distinct peptides, which impeded the data analysis. The obtained binding parameters, K_d and B_{max}, are shown in Table 4 and the saturation binding curves are included in Figure S3 in the Supporting Information (for non-specific binding curves and standard curves see Figures S4 and S5). It is worth noting that all novel TATE derivatives are highly potent SST_2 ligands with similar K_d (2.09−2.76 nM) and B_{max} values (256-586 fmol/mg) as the reference ligand **[^{64}Cu]Cu-NODAGA-TATE** (3.17 nM and 649 fmol/mg), even though a quite large structural N-terminal extension was introduced. In

addition to the SST_2 binding, the $logD_{7.4}$ values were determined revealing similar values within the series of **[^{64}Cu]Cu-NODAGA-NES(1-4)-TATEs** (between -2.13 and -2.60) but significantly higher than the partition coefficient of **[^{64}Cu]Cu-NODAGA-TATE** (-3.43).[47]

Overall, the radiopharmacological characterization of the **[^{64}Cu]Cu-NODAGA-NES(1-4)-TATEs**, in particular the high binding affinity to SST_2 and the sufficient stability in mouse plasma encouraged the further radiopharmacological characterization of the compounds *in vivo*.

Biodistribution of ^{64}Cu-labeled NODAGA-NES(1-4)-TATEs

The regional distribution of the **[^{64}Cu]Cu-NODAGA-NES(1-4)-TATEs** was analyzed in a subcutaneous MPC tumor allograft model via small-animal PET imaging (Figure 7 C-F). The kinetic profiles of activity uptake in tumor, kidneys, and liver are shown in Figure 8 C-F (for kinetic profiles of muscle and heart, see Figure S6 in Supporting Information) and the calculated areas under curves ($AUC_{0\text{-}24\ h}$) are graphically summarized in Figure 9 along with the respective tumor/tissue ratios. For comparison, PET data for **[^{64}Cu]Cu-NODAGA-TATE** and **[^{64}Cu]Cu-NODAGA-Pra-O2Oc-TATE**, which were recently characterized by us,[47] were included in Figure 7-8.

The kinetic profiles for the tumor uptake are similar among all compounds and reveal a fast accumulation in the MPC tumor with highest SUV peaks being reached at early time points *p.i.* (<30 min) followed by washout from the tumor. However, the achieved $AUC_{0\text{-}24\ h}$ values for the **[^{64}Cu]Cu-NODAGA-NES(1-4)-TATEs** (11.2-35.8) are significantly lower than the values for **[^{64}Cu]Cu-NODAGA-TATE** (124.8) and **[^{64}Cu]Cu-NODAGA-Pra-O2Oc-TATE** (58.9). In this context, the latter radioligand might serve as the better reference compound for tumor and kidney uptake than **[^{64}Cu]Cu-NODAGA-TATE** as already the insertion of the mini-PEG2 linker affects both. The tumor uptake is reduced by half and the reason for that appears to be an accelerated renal clearance as the highest SUV peaks in the kidneys are shifted to earlier time points *p.i.* leading to reduced $AUC_{0\text{-}24\ h}$ values (9.7 *versus* 30.7). In line with this, the activity increase in the bladder is faster for **[^{64}Cu]Cu-NODAGA-Pra-O2Oc-TATE** compared to **[^{64}Cu]Cu-NODAGA-TATE** (Figure S7 in Supporting Information). Consequently, the tumor/tissue ratios are quite similar between **[^{64}Cu]Cu-NODAGA-TATE** and **[^{64}Cu]Cu-NODAGA-Pra-O2Oc-TATE** (Figure 9 B).

The kinetic profiles of the **[^{64}Cu]Cu-NODAGA-NES(1-4)-TATEs** for the kidneys reveal, that the maximum SUV peaks (4.6-8.8*)* were considerably lower compared to **[^{64}Cu]Cu-NODAGA-Pra-O2Oc-TATE** (13.9). However, the $AUC_{0\text{-}24\ h}$ values were only lower for **[^{64}Cu]Cu-**

NODAGA-NES2-TATE (4.0) and **[^{64}Cu]Cu-NODAGA-NES3-TATE** (7.5), while **[^{64}Cu]Cu-NODAGA-NES1-TATE** (17.7) and **[^{64}Cu]Cu-NODAGA-NES4-TATE** (15.5) show higher values resulting from a slower washout. Regarding the uptake in the liver, the maximum SUVs in the liver were increased for the **[^{64}Cu]Cu-NODAGA-NES(1-4)-TATEs** (5.0-8.0) compared to **[^{64}Cu]Cu-NODAGA-Pra-O2Oc-TATE** (2.7), but the $AUC_{0\text{-}24\ h}$ values are similar ranging from 3.5 to 4.5. Considering the plasma stabilities of the **[^{64}Cu]Cu-NODAGA-NES(1-4)-TATEs**, a somewhat lower tumor accumulation of the novel TATE derivatives due to premature cleavage in the blood circulation could have been expected. Moreover, this premature cleavage could also explain the higher initial liver uptake as the small cleavage fragments might exhibit a different biodistribution than the intact peptides. Likewise, the **[^{64}Cu]Cu-NODAGA-NES(1-4)-TATEs** are more hydrophobic than **[^{64}Cu]Cu-NODAGA-TATE** and **[^{64}Cu]Cu-NODAGA-Pra-O2Oc-TATE**, which might also contribute to the altered liver uptake (Table 4). However, the trend in tumor and kidney uptake within the series of **[^{64}Cu]Cu-NODAGA-NES-TATEs** is surprising. In particular, **[^{64}Cu]Cu-NODAGA-NES1-TATE** shows by far the highest tumor uptake even though the stability in mouse plasma is comparable to the other peptides or even lower (Table 3).

Assessing the reasons for the observed uptake of the ^{64}Cu-labeled NODAGA-NES(1-4)-TATEs in kidneys and tumor

For explaining this phenomenon, a different degree of premature degradation of the radioligands than seen for the *in vitro* plasma incubations was considered. The possibility for a NEP-catalyzed cleavage at the tumor site was excluded based on immunohistochemical staining of MPC tumor slices. In this context, the high NEP levels in the kidneys of the mice were confirmed by this method (Figure S8 in Supporting Information). In addition to its high abundance in the renal brush border membrane, NEP is also present amongst others in the endothelium.[65, 66] In this context, the Marion de Jong and colleagues explored the concept of increasing the bioavailability of radiolabeled peptides by co-injection of enzyme inhibitors that degrade the peptides in the blood circulation. In particular, co-injection of phosphoramidon significantly increased the plasma half-life of radiolabeled minigastrin analogs in mice, which in turn led to a markedly increased tumor uptake.[67-70] The action of phosphoramidon might be explained by inhibition of not only soluble NEP but also of endothelium-derived NEP. Therefore, we concluded that the *in vitro* plasma half-lives might be overestimated in case of peptides acting as NEP substrates. To ascertain this hypothesis, human umbilical vein endothelial cells (HUVEC) were selected and the synthesis of NEP was confirmed via Western Blotting (Figure S9 in Supporting Information). Subsequently, the stability in the presence of

HUVEC was exemplarily studied for **[^{64}Cu]Cu-NODAGA-NES4-TATE** under different conditions (Figure S10 in Supporting Information). After 4 h, 5% (63% dose/mg) of the intact radioligand was cleaved to the respective cleavage fragment **[^{64}Cu]Cu-NODAGA-PAMBA-rG-OH**, which was completely blocked in the presence of phosphoramidon (0.1 µM) or thiorphan (0.1 µM, Figure 4), but not in the presence of captopril (10 µM). Thiorphan was included in this experiment as it is a more selective inhibitor of NEP than phosphoramidon, as the latter exhibits some cross-reactivity with endothelin converting enzyme 1 (ECE1),[71] which is another member of the M13 family. ECE-1 shares the cleavage site specificity of NEP and is also present on endothelial cells but is not inhibited by thiorphan.[72-74] Therefore, a contribution of endothelium-derived NEP to the degradation of the **[^{64}Cu]Cu-NODAGA-NES(1-4)-TATEs** appears likely.

To demonstrate that the *in vitro* plasma half-lives are overestimated, an *ex vivo* metabolite analysis of **[^{64}Cu]Cu-NODAGA-NES4-TATE** (in blood, liver, kidney, and urine) after *i.v.* injection in healthy mice was performed (Figure 10). Accordingly, the blood analysis revealed that 5 min *p.i.* only 19% and 15 min *p.i.* only 4% of the residual activity in the blood circulation belongs to the parent peptide while the majority can be assigned to **[^{64}Cu]Cu-NODAGA-PAMBA-rG-OH**, the same radiolabeled metabolite, which was observed upon incubation with recombinant NEP, on HUVEC, and in human and mouse plasma (*in vitro*). Consequently, the *in vivo* blood half-life of **[^{64}Cu]Cu-NODAGA-NES4-TATE** amounts to less than 5 min, which is significantly lower than the half-life determined for the *in vitro* mouse plasma incubation (450 min). This in turn strongly emphasizes that endothelium-derived NEP, in addition to soluble NEP, contributes to the overall NEP activity in the blood circulation. The lower tumor uptake of **[^{64}Cu]Cu-NODAGA-NES(2-4)-TATE** compared to **[^{64}Cu]Cu-NODAGA-NES1-TATE** appears now comprehensible due to their higher substrate potential toward NEP (Table 3). In this context, for **[^{64}Cu]Cu-NODAGA-NES1-TATE** and **[^{64}Cu]Cu-NODAGA-NES2-TATE**, the cleavage by other proteases was observed in mouse plasma incubations, but their contribution to the overall in vivo stability appears not to be predominant.

Considering the pronounced premature cleavage of the radioligands in the blood circulation, the derivation of a rationale for the observed kidney uptake of the **[^{64}Cu]Cu-NODAGA-NES(1-4)-TATEs** is complicated. Basically, the cleavage of residual intact **[^{64}Cu]Cu-NODAGA-NES4-TATE** that enters the proximal tubule by renal NEP can be deduced from the *ex vivo* metabolite data, as 5 min *p.i.* no parent peptide was detectable in the kidney and urine (Figure 10). For **[^{64}Cu]Cu-NODAGA-NES1-TATE** and **[^{64}Cu]Cu-NODAGA-NES2-TATE**, the analysis of urine samples by RP-HPLC 2 h *p.i.* similarly revealed the complete degradation of the parent peptides to the expected radiolabeled cleavage fragments (Figure S11 in Supporting Information). Accordingly, even the substrate potential of **[^{64}Cu]Cu-NODAGA-NES1-TATE**

(k_{obs}/[E] of 1,950 $M^{-1}s^{-1}$), which is the lowest of the **[^{64}Cu]Cu-NODAGA-NES-TATEs** studied herein, appears sufficient for a fast cleavage in the kidneys. Apart from the cleavage rate, the differences in kidney uptake might be at least partially affected by the different cleavage fragments itself and their elimination behavior. In this context, **[^{64}Cu]Cu-NODAGA-NES2-TATE** and **[^{64}Cu]Cu-NODAGA-NES3-TATE**, which show the lowest kidney uptake, are metabolized to the cleavage fragments **[^{64}Cu]Cu-NODAGA-PAMBA-Nle-OH** and **[^{64}Cu]Cu-NODAGA-PAMBA-G-OH**, respectively. These radiometabolites resemble the structure of hippuric acid (*N*-Benzoylglycine), which undergoes a fast renal elimination due to glomerular filtration and tubular secretion.[75] Furthermore, as mentioned in the introduction, 3′-[^{131}I]iodohippuric acid was identified as fast eliminating species from a 3′-[^{131}I]iodohippuryl N^{ε}-maleoyl-lysine ([^{131}I]HML)-labeled Fab.[27] In contrast, the cleavage fragments of **[^{64}Cu]Cu-NODAGA-NES1-TATE** and **[^{64}Cu]Cu-NODAGA-NES4-TATE**, *i.e.* **[^{64}Cu]Cu-NODAGA** / **[^{64}Cu]Cu-NODAGA-Nle-OH** and **[^{64}Cu]Cu-NODAGA-PAMBA-rG-OH**, lack the aromatic moiety or bear an additional positive charge, which could affect their elimination behavior.

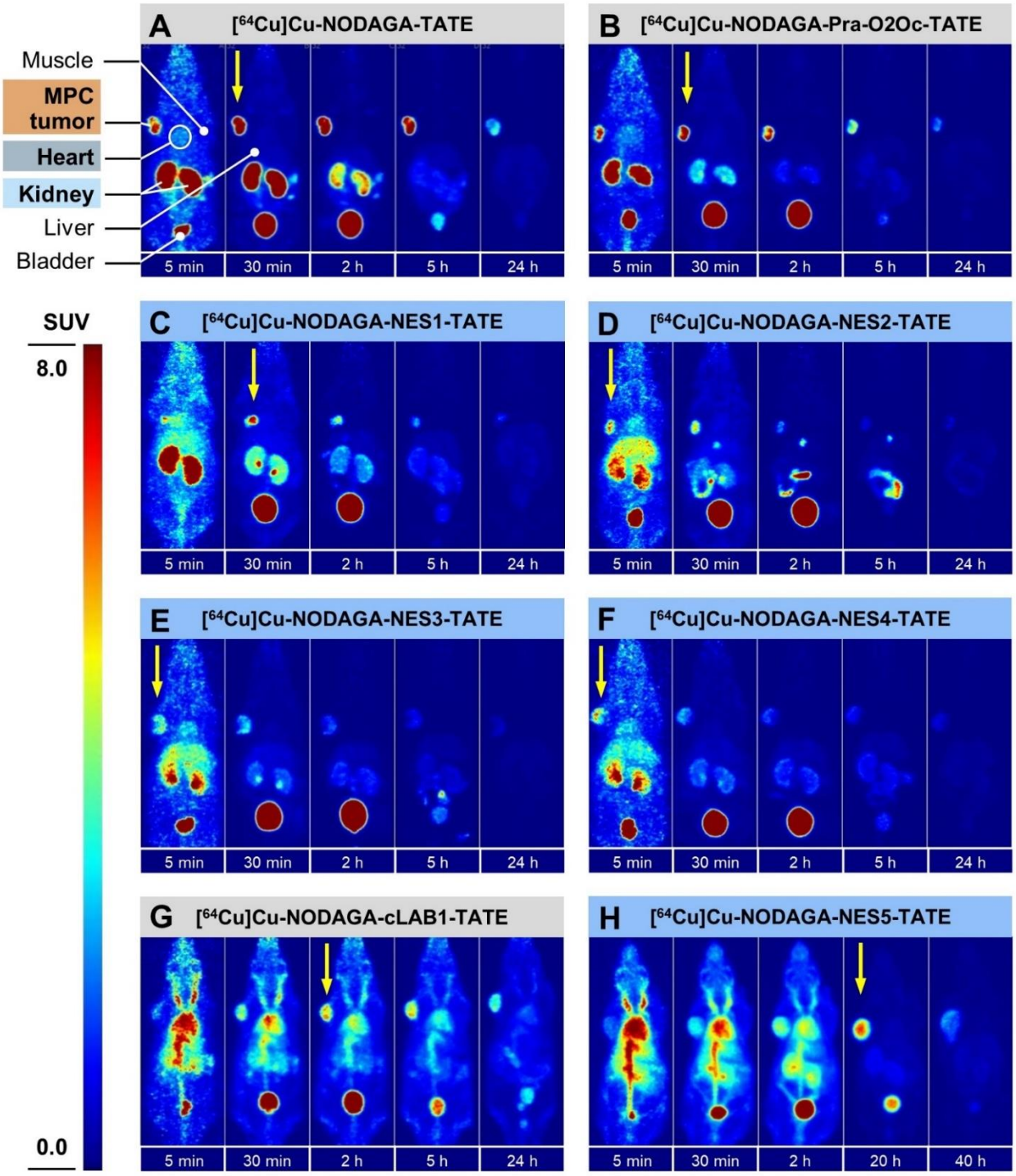

Figure 7. PET images for the ^{64}Cu-labeled NODAGA-NES-TATEs.

PET images (A−H) at selected time points after intravenous injection of the different ^{64}Cu-labeled compounds (7−10 MBq/animal) in MPC tumor-bearing mice. Images are presented as maximum intensity projections and shown at a common scale. Anatomical positions of tumor, heart, kidney, liver, and muscle used for SUV quantification are exemplarily shown for **[^{64}Cu]Cu-NODAGA-TATE** (A). Vertical arrows indicate time points with the highest tumor uptake. Indicated time points correspond to the following time frames: 5 min [4−6 min], 30 min [25−40 min], 2 h [105−120 min], 5 h [4.5−5.5 h], 20 h [19-21 h], 24 h [23−25 h], and 40 h [39-41 h]. PET images for **[^{64}Cu]Cu-NODAGA-TATE**, **[^{64}Cu]Cu-NODAGA-Pra-O2Oc-TATE** and **[^{64}Cu]Cu-NODAGA-cLAB1-TATE** were previously published.[47]

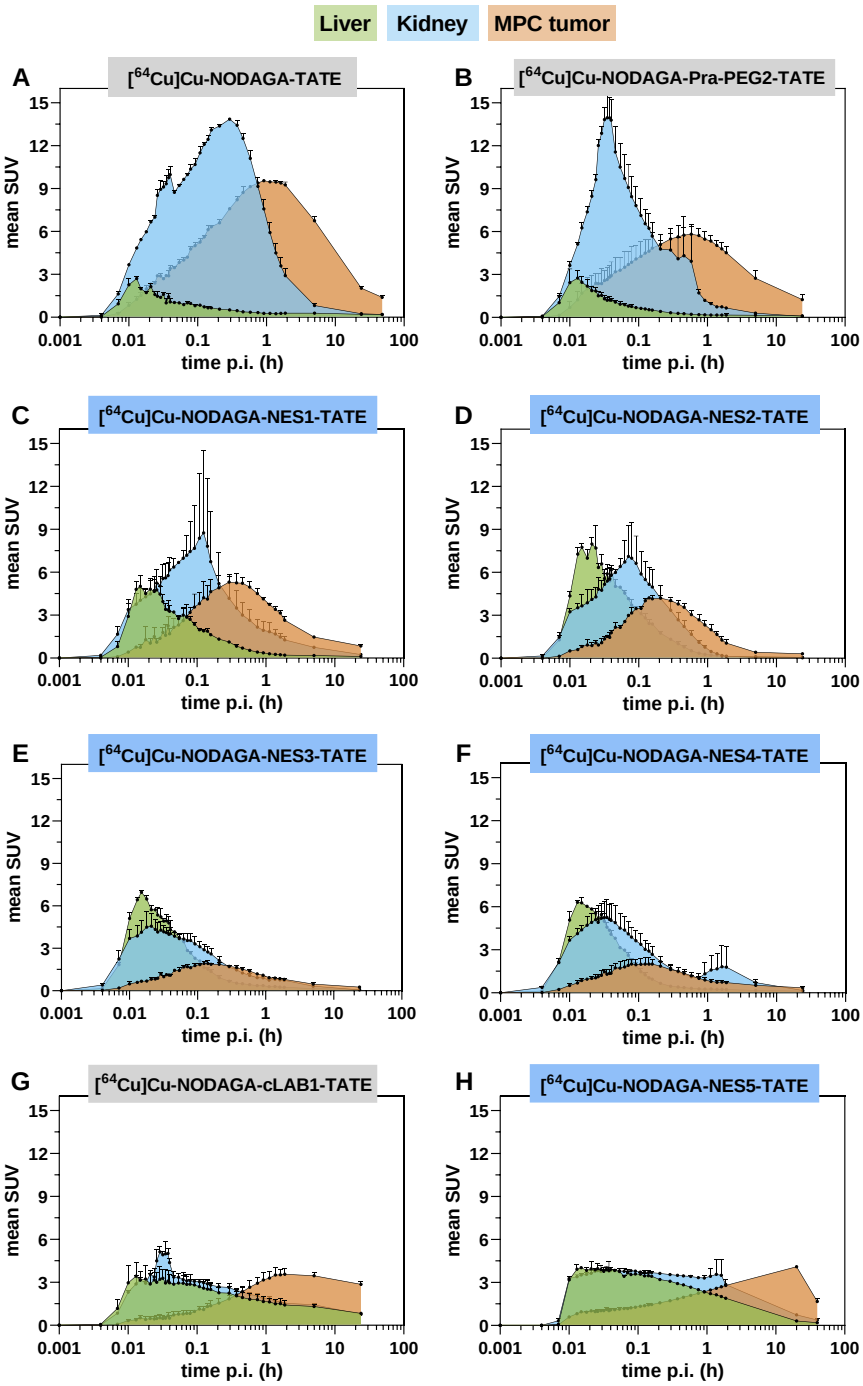

Figure 8. Time-dependent SUV data of liver, kidney, and MPC tumor for the ^{64}Cu-labeled NODAGA-NES-TATEs.

In (**A**–**H**), standard uptake values (SUV, decay-corrected) as a function of time (up to 24 or 48 h) obtained by PET acquisition (0–2 h in dynamic mode and time points 5, 24, and 48 h *p.i.* For **[^{64}Cu]Cu-NODAGA-NES5-TATE**, time points were slightly different (0–2 h in dynamic mode and time points 20 and 40 h *p.i.*; x-axes are shown in logarithmic scale. Data shown are mean values of a group of MPC tumor-bearing NMRI-nu/nu mice (n =2–3). The area under the respective curves was filled with color for a better visualization (same color code as in ref. [47]). Data for **[^{64}Cu]Cu-NODAGA-TATE**, **[^{64}Cu]Cu-NODAGA-Pra-O2Oc-TATE** and [^{64}Cu]**Cu-NODAGA-cLAB1-TATE** were previously published and compound names were colored in grey compared to the blue coloring of the novel NES-TATEs.[47]

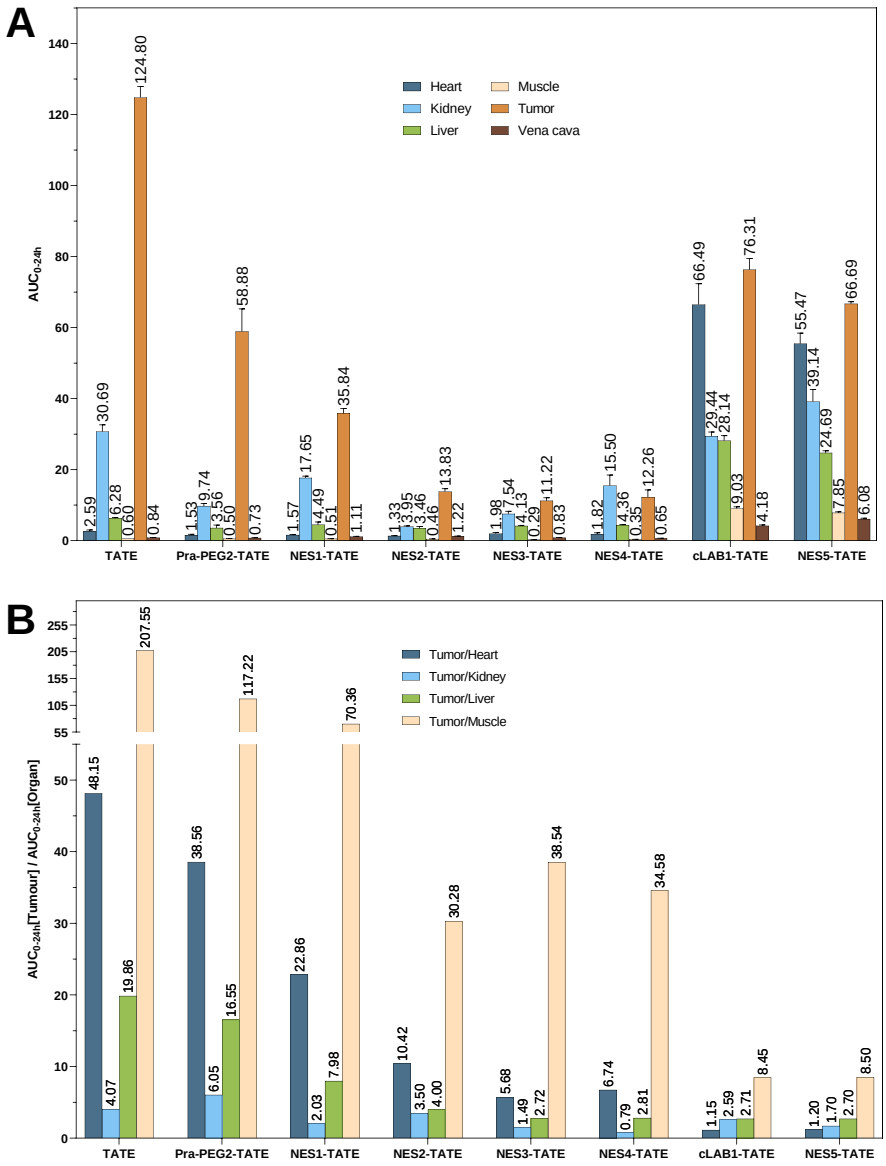

Figure 9. Summary of calculated $AUC_{0-24\ h}$ values and the respective tumor/organ ratios

(**A**, **B**) Calculated $AUC_{0-24\ h}$ values (but $AUC_{0-20\ h}$ for NES5-TATE) and the tumor/organ ratios for the different ^{64}Cu-labeled TATE derivatives. For a better overview, the compound names were abbreviated. Data shown in (A) are mean values (±SD). Data for [**^{64}Cu]Cu-NODAGA-TATE**, **[^{64}Cu]Cu-NODAGA-Pra-O2Oc-TATE** and [**^{64}Cu]Cu-NODAGA-cLAB1-TATE** were previously published.[47]

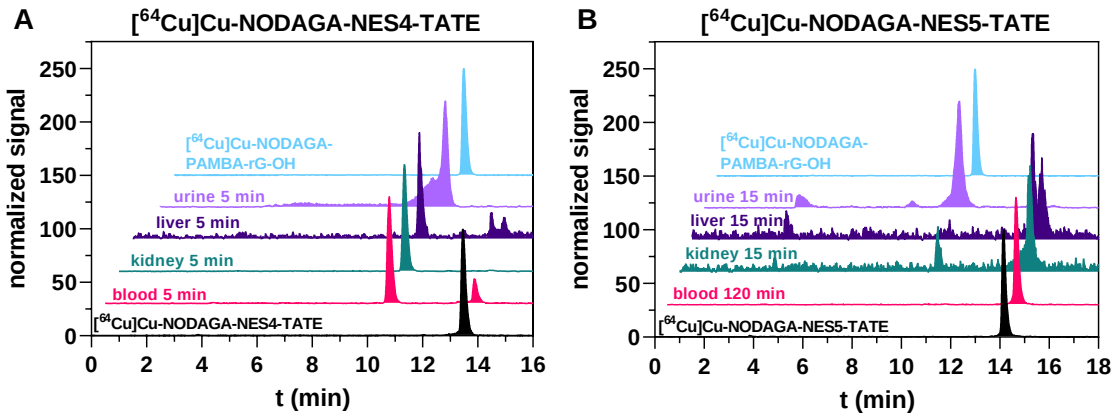

Figure 10. Ex vivo metabolite analysis for [^{64}Cu]Cu-NODAGA-NES4-TATE and [^{64}Cu]Cu-NODAGA-NES5-TATE

(**A/B**) Exemplary HPLC chromatograms of **[^{64}Cu]Cu-NODAGA-NES4-TATE** (black, t_R=13.4 min) and **[^{64}Cu]Cu-NODAGA-NES5-TATE** (black, t_R=14.1 min), the cleavage fragment **[^{64}Cu]Cu-NODAGA-PAMBA-rG-OH** (blue, t_R=10.4 min) and for samples of blood (pink), kidney (green), liver (purple), and urine (light purple) taken 5 min after *i.v.* injection of **[^{64}Cu]Cu-NODAGA-NES4-TATE** and **[^{64}Cu]Cu-NODAGA-NES5-TATE** in a healthy NMRI-nu/nu mouse. Note, HPLC traces are shifted (0.5 min at the x-axis and 30 units at the y-axis).

Characterization of the triple-targeting radioligand [^{64}Cu]Cu-NODAGA-NES5-TATE

Considering the PET data and the results of the *ex vivo* metabolite analysis, it became clear that the introduction of a NEP-directed cleavage sequence into vector molecules entails a lower plasma stability due to the presence of NEP in the blood circulation (soluble and endothelium-based). In line with our results are *ex vivo* metabolite data from Bendre *et al.* for ^{68}Ga-labeled PSMA ligands bearing **DOTA-PAMBA-MVK-OH** as cleavable linker, even though the authors did not mention a NEP-catalyzed cleavage in the blood.[44] Moreover, the free C-terminus in that cleavable linker might entail cleavage by ACE in the blood circulation. Accordingly, the tumor uptake is significantly lowered compared to the respective PSMA ligand without cleavable linker (^{68}Ga-HTK01166).[76] In contrast, premature cleavage in the blood circulation is apparently not an issue for large vector molecules such as exendin-4[39, 42] or Fabs[31] that usually bear NOTA-Bn-NCS functionalized cleavable linkers. Considering the kinetic data presented herein on the cleavage of NEP substrates with N-terminal (thio)urea functionality, this might rely primarily on the low substrate potential of these compounds toward NEP compared to peptides with N-terminal amide group. In addition to that, an important structural feature for NEP is the size-restricted active site, for which the access is limited to substrates <3 kDa rendering this enzyme rather an oligopeptidase than a protease.[34, 77, 78] Accordingly, the cleavability of functionalized Fabs (~50 kDa) or exendin-4 (~4 kDa) by NEP is at least questionable and would actually be required to assess (as done herein for the TATE

derivatives with recombinant NEP). Instead, model substances such as **Boc-MVK(Dde)-OH**[42], **[^{67}Ga]Ga-NOTA-Bn-NCS-MVK(Benzoyl)-OH**[30] or **^{99m}Tc-MAG3-GFK(4-(benzylamino)-4-oxobutanoyl)**[79] were usually employed to demonstrate the susceptibility to a NEP-catalyzed degradation with BBMVs as source for NEP.

Considering the restricted active site of NEP, we developed the idea to mask the susceptibility to a NEP-catalyzed cleavage in the blood circulation by functionalizing the **NODAGA-NES-TATEs** with an albumin binder. The albumin-bound peptide should not be recognized as substrate by NEP and thus, the rate of degradation in the blood circulation is lowered. However, the targeting of NEP at the brush border membrane might not be affected as the albumin concentration in the ultrafiltrate is dramatically lowered (fractional filtration around 0.1%).[80-82] For this purpose, the sequence of **NODAGA-NES4-TATE** was chosen and the introduction of the "clickable" albumin binder *N*$^{\alpha}$-(4-Pentynoyl)-*N*$^{\varepsilon}$-(4-(4-iodophenyl)butanoyl)-L-lysine via CuAAC was envisaged.[47] The resulting **NODAGA-NES5-TATE** (Figure 5) was analogously synthesized as compounds **NODAGA-NES(1-4)-TATE** with the on-resin CuAAC following the introduction of NODAGA (Scheme S2 in Supporting Information). The analytical data for this compound and its ^{64}Cu-labeled analog are included in Table 1-3. Worth of note, **[^{64}Cu]Cu-NODAGA-NES5-TATE** exhibits a high substrate potential (k_{obs}/[E]=42,800 $M^{-1}s^{-1}$), even though a large moiety was introduced at the Lys(N_3) residue, but the value is lower compared to **[^{64}Cu]Cu-NODAGA-NES4-TATE** (109,000 $M^{-1}s^{-1}$). The albumin-binding affinity has been determined to be 3.2 µM using a recently described radiometric ultrafiltration assay (Figure S12 in Supporting Information).[47] To demonstrate the stabilizing effect of albumin on the cleavage rate by NEP, the radiometric NEP assay was also performed in the presence of 150 µM human serum albumin (HSA), which means that approx. 98% of the radioligand is bound to HSA.[47] The cleavage under these conditions proceeded considerably slower with an apparent k_{obs}/[E] of 5,400 $M^{-1}s^{-1}$ (factor of 8, Figure S1 in Supporting Information). However, after 24 h the cleavage is almost quantitative, which is comprehensible due to the reversible binding of **[^{64}Cu]Cu-NODAGA-NES5-TATE** to albumin. In line with these results, **[^{64}Cu]Cu-NODAGA-NES5-TATE** is almost completely stable in human and mouse plasma over 24 h.

The regional distribution of **[^{64}Cu]Cu-NODAGA-NES5-TATE** was analyzed in the same manner as done for the **[^{64}Cu]Cu-NODAGA-NES(1-4)-TATEs**. The respective data are included in Figure 7-8 together with the previously published data for the albumin-binding TATE derivative **[^{64}Cu]Cu-NODAGA-cLAB1-TATE**, which has a similar binding affinity to albumin (K_d of 3.1 µM) but lacks the cleavable linker for NEP.[47] The PET data for **[^{64}Cu]Cu-NODAGA-NES5-TATE** reveal, that for all organs including the tumor the kinetic profiles resemble those of **[^{64}Cu]Cu-NODAGA-cLAB1-TATE**. In particular, the blood circulation time

is prolonged compared to the TATE derivates without albumin-binding moiety, as seen by the time-dependent SUV data for the heart (Figure S6 in Supporting Information). Consequently, the tumor uptake is protracted, which reflects the binding to albumin in the blood and thus, the lowering of the unbound fraction of the radioligand. Nevertheless, the $AUC_{0\text{-}24\ h}$ value for **[^{64}Cu]Cu-NODAGA-cLAB1-TATE** (76.3) and the $AUC_{0\text{-}20\ h}$ value for **[^{64}Cu]Cu-NODAGA-NES5-TATE** (66.7) exceed the $AUC_{0\text{-}24\ h}$ values for the other mini PEG2 linker-bearing TATE derivates (11.2-58.9), which most likely originate from an additional tumor uptake of the albumin-bound radioligand.[47, 83]

The comparison of **[^{64}Cu]Cu-NODAGA-NES4-TATE** and **[^{64}Cu]Cu-NODAGA-NES5-TATE** is striking as both compounds share the cleavable linker motif for NEP (-PAMBA-rGFK(X)-), but the tumor uptake of the latter radioligand is 5-times higher than that of the former. Apart from the effect of the albumin binder on the tumor uptake, this strongly indicates that the stability of **[^{64}Cu]Cu-NODAGA-NES5-TATE** is increased compared to **[^{64}Cu]Cu-NODAGA-NES4-TATE**. To prove that, an *ex vivo* metabolite analysis was performed for **[^{64}Cu]Cu-NODAGA-NES5-TATE** (Figure 10 B). This revealed that the radioligand remains stable in the blood circulation even 2 h *p.i.* However, even though the cleavage fragment **[^{64}Cu]Cu-NODAGA-rG-OH** was not detected in the *ex vivo* analysis of the blood, the small fraction of unbound radioligand is certainly processed by NEP, which accounts for a faster blood clearance and higher tumor-to-heart ratios of **[^{64}Cu]Cu-NODAGA-NES5-TATE** compared to **[^{64}Cu]Cu-NODAGA-cLAB1-TATE** at time points >20 h *p.i.* (Figure S13 in Supporting Information). In contrast to the blood, **[^{64}Cu]Cu-NODAGA-rG-OH** was found in the kidneys and even exclusively in the urine 15 min *p.i.* This clearly highlights, that the approach of masking the NEP recognition in the blood circulation by albumin binding without impairing the cleavage at the renal brush border is working. Although the targeting of renal NEP is achieved with **[^{64}Cu]Cu-NODAGA-NES5-TATE**, the kidney uptake is apparently not lowered compared to **[^{64}Cu]Cu-NODAGA-cLAB1-TATE**, which could be related to the potentially unfavorable properties of the cleavage fragment **[^{64}Cu]Cu-NODAGA-PAMBA-rG-OH** (see discussion above).

The data presented herein, in particular the comparison between unbound and albumin-bound radioligand, led us to elaborate simplified models that describe the *in vivo* fate of different target molecules bearing cleavable linkers for NEP, ranging from small molecules or peptides to proteins (Figure 11).

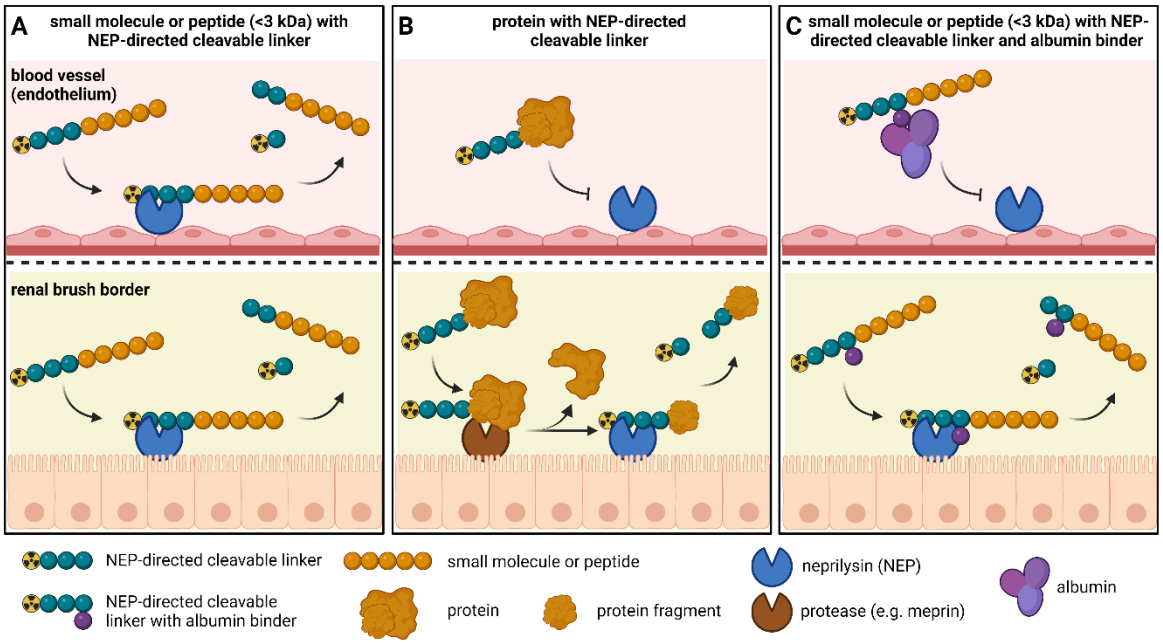

Figure 11. Proposed models for the in vivo fate of different radioligands bearing cleavable linkers for NEP

A) Small molecules and peptides that fit the size restriction for the active site of NEP (<3 kDa), e.g. **[^{64}Cu]Cu-NODAGA-NES(1-4)-TATEs**, are cleaved by NEP in the blood circulation (soluble and membrane bound on endothelial cells). Compounds with higher substrate potential are faster cleaved, which in turn affects radioligand binding to the actual target at the tumor site (herein, SST_2). Residual intact radioligand is cleaved after glomerular filtration at the renal brush border membrane by NEP. **B**) Proteins functionalized with cleavable linkers for NEP, e.g. Fabs (~50 kDa), are too large to be recognized by NEP as substrates and remain stable in the blood circulation, irrespective of the actual substrate potential of the isolated cleavable linker. Once the protein enters the proximal tubule, it appears likely that other proteases, e.g. meprin A, predigest the radiolabeled protein resulting in the formation of at least one radiolabeled fragment whose size now enables the action of NEP. In this context, known substrates of meprin A are Insulin and exendin-4.[84-87] It is worth noting that BBMVs also contain meprin A.[88] **C**) Small molecules and peptides that are equipped with an albumin binder (besides bearing a cleavable linker for NEP), e.g. **[^{64}Cu]Cu-NODAGA-NES5-TATE**, are not cleaved in the blood circulation as the albumin complex is too large for being processed by NEP. The binding affinity to albumin determines the magnitude of the albumin-bound fraction. Due to significant lower concentration of albumin in the proximal tubule, the equilibrium of albumin binding is shifted and the unbound radioligand is cleaved by NEP. Figure was created with Biorender.com.

Conclusion

The present study is focused on the emerging strategy of lowering the kidney uptake of targeted radiopharmaceuticals by generating fast eliminating cleavage fragments upon NEP-catalyzed cleavage at the brush border membrane in the proximal tubule. For the first time, the substrate potential of ^{64}Cu-labeled cleavable linkers toward NEP was quantified by a radiometric HPLC assay. This led to the discovery that GFK-derived cleavable linkers are generally more potent NEP substrates than linkers based on MVK. Furthermore, an N-terminal aromatic residue, such as PAMBA, increases the substrate potential, while an N-terminal (thio)urea functionality exerts the opposite effect. Likewise, the particular structure of the cleavable linker affects the specificity toward NEP with C-terminally amidated analogs being

more resistant toward the activity of ACE and an additional D-Arg residue confers even complete specificity. These findings ended in the design of the **[^{64}Cu]Cu-NODAGA-NES(1-4)-TATEs**, in which the NEP-directed cleavage sequence is placed as N-terminal elongation of the actual target molecule TATE. The respective substrate potentials toward NEP range from 1,950 to 109,000 $M^{-1}s^{-1}$. The radiopharmacological characterization of the series of **[^{64}Cu]Cu-NODAGA-NES(1-4)-TATEs** actually aimed at studying the kidney uptake in dependence on the particular substrate potentials, but uncovered the phenomenon of a pronounced premature cleavage in the blood circulation, which is predominantly caused by the activity of endothelium-derived NEP. Based on the structural features of NEP's active site, that limits the access to rather small molecules (<3 kDa), we achieved an exclusive cleavage by NEP in the kidneys for compound **[^{64}Cu]Cu-NODAGA-NES5-TATE** due to reversible albumin binding in the blood circulation. This renders the triple-targeting approach (SST_2, NEP and albumin) a new strategy for masking the recognition by NEP in the blood circulation, which is of particular importance for small molecules or peptides. Likewise, albumin-binding radioligands could benefit from NEP-directed cleavable linkers to reduce the often-observed higher kidney uptake compared to analogues radioligands without albumin binder.

Based on the presented data, we conclude that for an efficient cleavage by NEP in the kidneys already moderate to low substrate potentials, such as that of **[^{64}Cu]Cu-NODAGA-NES1-TATE** (k_{obs}/[E] of 1,950 $M^{-1}s^{-1}$), are sufficient. Consequently, the incorporation of a cleavable linker that bears a urea functionality at the N-terminus is obvious to investigate the relation of NEP cleavage in the blood and in the kidneys for a compound with even lower substrate potential. However, a specific targeting of NEP in the kidneys might not be possible for small molecules or peptides. The reversible binding to albumin appears an exciting approach to solve this problem and we assume that this approach is worth to advance.

Experimental Section

General

All commercial reagents and solvents were used without further purification unless otherwise specified. For the incorporation of NODAGA, the building (*R*)-NODA-GA(tBu)$_3$ (CheMatech) was used. Mass spectra (ESI) were obtained on a Waters Xevo TQ-S mass spectrometer driven by the Mass Lynx software. All regression analyses were done with GraphPad Prism (version 9.1.2, GraphPad Software, San Diego, CA, USA). The purity of compounds **1**-**6** and **NODAGA-NES(1-5)-TATEs** proved to be ≥ 95% as analyzed by analytical HPLC.

Chromatography

The HPLC system used was a LC-20A Prominence HPLC by Shimadzu, consisting of degasser unit DGU-20A5R, two separate pumping units LC-A20R, sample manager SIC-20ACHT, column oven CTO-20AC, PDA-detector SPD-M20A, communication-bus module CBM-20A and fraction collector FRC-10A. Two Aeris Peptide 5 µm XB-C18 columns (100 Å, 250x4.6 mm and 250x21.2 mm) were used as the stationary phases for analytical and preparative RP-HPLC, respectively. A binary gradient system of 0.1% CF_3COOH/water (solvent A) and 0.1% CF_3COOH/CH_3CN (solvent B) at a flow rate of 1 mL/min (analytical) or between 10-20 mL/min (preparative) served as the eluent. High resolution mass spectra (HRMS) were obtained on a Q-TOF MS using electrospray ionization: Agilent 1260 Infinity II HPLC (Santa Clara, California, USA; pump G7111B, autosampler G7129A, column oven G7116N, UV detector G7717C, eluent CH_3CN/water acidified with 0.1% formic acid 80/20, bypass mode) coupled to UHD Accurate Mass Q-TOF LC MS G6538A. Unless otherwise stated, the measurements were performed in bypass mode using an eluent consisting of (A): 0.1 % formic acid in CH_3CN and (B): 0.1% formic acid in H_2O; flow rate 0.25 mL/min. A reference mass solution containing ammonium trifluoroacetate, hexakis(1H,1H,3H-tetrafluoropropoxy)phosphazene, and purine was continuously co-injected via dual ESI source. For UPLC-DAD-MS, a system from Waters (ACQUITY UPLC I class system including a ACQUITY UPLC PDA e λ detector coupled to a Xevo TQ-S mass spectrometer) was used. A ACQUITY UPLC BEH C18 column (1.7 µm, 130 Å, 100x2.1 mm, equipped with a ACQUITY UPLC BEH C18 VanGuard Pre-column, 1.7 µm, 130 Å, 5x2.1 mm) was used as stationary phase. A binary gradient system of 0.1% CH_3COOH/water (solvent A) and 0.1% CH_3COOH in CH_3CN/CH_3OH (1:1, v/v, solvent B) at a flow rate of 0.4 mL/min served as the eluent. Analytical radio-HPLC was performed on a Series 1200 device (Agilent Technologies, Santa Clara, CA, USA) equipped with a Ramona ß/γ-ray detector (Raytest, Straubenhardt, Germany). Eluent A:

0.1% (v/v) trifluoroacetic acid in H_2O; eluent B: 0.1% (v/v) trifluoroacetic acid in acetonitrile; HPLC system: Zorbax SB-C18, 300 Å, 4 µm, 250 × 9.4 mm (Agilent); gradient elution using 95% eluent A for 5 minutes, 95% eluent A to 95% eluent B in 10 minutes, 95% eluent B for 5 minutes and 95% eluent B to 95% eluent A in 5 minutes, 3 mL/minute, 50 °C, recovery of activity (decay-corrected) was > 95 %.

Synthetic procedures

All syntheses were performed as solid-phase syntheses. Furthermore, the **GPs II**, **III**, **IV** and **VIII** were performed in an automated microwave peptide synthesizer (Initiator+ Alstra from Biotage®).

GP I: General procedure for loading of the 2-ClTrtCl resin

2-ClTrtCl resin (Iris-Biotech, 142 mg, 0.2 mmol, 1.4 mmol/g) was weight into a syringe with frit and suspended in CH_2Cl_2 (1 mL/0.1 mmol) for 30 min. Subsequently, DIPEA (70 µL, 0.4 mmol, 2 eq.) and the respective Fmoc-protected amino acid (0.125 mmol, 0.625 eq.) were added. The suspension was shaken for 2 h. The resin was washed with 2 ml of CH_2Cl_2 two times, followed by the addition of 5% MeOH in CH_2Cl_2 (2 mL, 1 mL/0.1 mmol) and DIPEA (350 µl, 2 mmol, 10 eq.). The resin was shaken for 30 min. The resin was washed with DMF, CH_2Cl_2, CH_3OH and diethyl ether (two times each). The resin was dried under suction for 5 min followed by 30 min at 55°C in an oven. The loading was determined by weighing of the resin.

GP II: General procedure for loading of the Rink Amide resin

Rink-amide resin (Fmoc-protected, Biotage, 260 mg, 0.2 mmol, 0.71 mmol/g) was weight into a syringe with frit and suspended in DMF (2 mL/0.1 mmol) with oscillating mixing and microwave heating (70°C) for 30 min. Fmoc removal was done by two cycles of 20% piperidine in DMF (4 mL, 2 mL/0.1 mmol) for 10 min each. The resin was washed with DMF twice and HATU (227 mg, 0.6 mmol, 3 eq., 0.5 M in DMF), DIPEA (210 µL, 1.2 mmol, 6 eq., 2 M in NMP) and Fmoc-Lys(N_3)-OH (237 mg, 0.6 mmol, 3 eq., 0.2 M in DMF) were added. The coupling was performed with oscillating mixing and microwave heating (75°C) for 5 min. After that the resin was washed with DMF twice.

GP III: General procedure for Fmoc removal

The resin was swollen in DMF (2 mL/0.1 mmol). Fmoc removal was done by two cycles of treatment with 20% piperidine in DMF (2 mL/ 0.1 mmol, 10 min each). After that, the resin was washed with DMF twice.

GP IV: General procedure for amino acid coupling

To the swollen resin, the respective Fmoc-protected amino acid (4 eq., 0.2 M in DMF), DIPEA (8 eq., 2 M in NMP) and HATU (4 eq., 0.5 M in DMF) were added. The coupling was performed with oscillating mixing and microwave heating (75°C) for 5 min. Subsequently, the resin was washed with DMF twice. In case of (*R*)-NODA-GA(tBu)$_3$, only 2, 4, and 2 eq. of (*R*)-NODA-GA(tBu)$_3$, DIPEA, and HATU, respectively were used.

GP V: General procedure for manual NODAGA coupling

To the swollen resin (0.03 mmol) in DMF (2 mL/0.1 mmol), (*R*)-NODA-GA(tBu)$_3$ (1 eq., 0.2 M in DMF), DIPEA (0.06 mmol, 11 µl, 2 eq.) and HATU (1 eq., 0.5 M in DMF) were added. The mixture was shaken at 750 rpm for 2 h. The resin was washed with DMF, CH_2Cl_2, CH_3OH and diethyl ether (two times each). The resin was dried under suction for 5 min followed by 30 min at 55°C in an oven.

GP VI: General procedure for NOTA-Bn-NCS coupling

The resin (0.1 mmol) was swollen in CH_2Cl_2 (2 mL/0.1 mmol). The peptide was cleaved with a mixture of HFIP in CH_2Cl_2 (1 mL/0.1 mmol, 1:4, v/v) for 5 min. This treatment was two times repeated. The combined fractions were dried in a flow of nitrogen. The residue was dissolved in DMF (200 µL) and NOTA-Bn-NCS (1 eq., 0.2 M in DMF) and DIPEA (0.1 mmol, 20 µL, 2 eq.) were added. The reaction was shaken at 750 rpm for 2 h. The residue was diluted with water (2 mL) and purification was performed by RP-HPLC.

GP VII: General procedure for the cleavage from the resin

To the dry resin (0.2 mmol, 0.7 mmol/g), TRIS (25 µL/0.1 mmol) and H_2O (25 µL/0.1 mmol) were added followed by TFA (1 mL/0.1 mmol). The resin was shaken for 30 min. The eluate and an additional volume TFA (0.5 mL/0.1 mmol) for washing were collected and dried under

reduced pressure and N_2 flow. The residue was dissolved in 50% CH_3CN/water and purified by RP-HPLC.

GP VIII: On-resin cyclization (disulfide formation)

Fully protected TATE was cyclized on-resin by the addition of iodine (10 eq.) in DMF (0.5 M). The suspension was shaken for 1 h.[89] After washing with DMF twice, the Fmoc group was removed by treatment with 20% piperidine in DMF for 10 min (2 cycles).

On-resin formation of the urea linkage in compound **5**

4-(*N*-Fmoc-aminomethyl)aniline (50 mg, 0.145 mmol, 3 eq.) and 4-nitrophenyl chloroformate (29 mg, 0.145 mmol, 3 eq.) were placed in a 1.5 ml tube and dissolved in 1 ml CH_2Cl_2. After addition of DIPEA (25 µl, 0.145 mmol, 3 eq.), the mixture was shaken for 30 min. The pre-activated solution was then added to a 2 ml syringe with frit, containing the swollen resin (0.05 mmol, NH_2-NleVK(N_3)-O-resin) in 0.5 ml CH_2Cl_2, DIPEA (51 µl, 0.29 mmol, 6 eq.) and a catalytic amount of DMAP (0.5 mg, 0.005 mmol, 0.1 eq.). The reaction was shaken for 4 h followed by washing with CH_2Cl_2 and DMF two times each.

On-resin copper-catalyzed azide-alkyne cycloaddition (CuAAC) for compound **NODAGA-NES5-TATE**

The peptide resin (30 µmol) was swollen in DMF (3 mL/0.1 mmol) for 30 min. After filtration of excessive DMF, the N^{α}-(4-Pentynoyl)-N^{ε}-(4-(4-iodophenyl)butanoyl)-L-lysine (17 mg, 30 µmol, 1 eq., synthesized according to our previously published procedure[47]) in DMF (2 mL), $CuSO_4$*$5H_2O$ (4 mg, 15 µmol, 0.5 eq.) and THPTA (7 mg, 15 µmol, 0.5 eq.) in water (245 µL) were added and shaken before addition of sodium ascorbate (29 mg, 150 µmol, 5 eq.) in water (105 µL). The suspension was shaken for 2 h. After elution, the resin was washed with DMF (20 mL), sodium diethyldithiocarbamate in DMF (0.5% w/v, 30 mL), DMF (20 mL), CH_2Cl_2 (20 mL), CH_3OH (20 mL) and diethylether (20 mL). The resin was finally dried at 55°C for 30 min in an oven.

Radiolabeling of NODAGA-bearing peptides

[^{64}Cu]$CuCl_2$ was produced at the Helmholtz-Zentrum Dresden-Rossendorf on the 30 MeV TR-Flex-cylotron (Advanced Cyclotron Systems Inc., ACSI, Canada) by the ^{64}Ni(p,n)^{64}Cu nuclear reaction as reported previously.[90, 91]

Radiolabeling was conducted as recently described.[47] Labeling yields were usually ≥97%. The radiolabeled peptides were used without purification. Molar activities of up to 50 GBq/µmol were achieved and were calculated based on the applied peptide amount. For further cell experiments and in vivo application, the reaction mixture was diluted with cell culture medium, phosphate-buffered saline (PBS, pH 7.4) or 0.154 M NaCl.

n-Octanol/PBS Distribution Coefficient ($logD_{7.4}$ value)

The determination of the $logD_{7.4}$ value was done as recently described.[47]

NEP cleavage assay

To 157.5 µL PBS (pH 7.4) were added 42.5 µL of the ^{64}Cu-labeled peptide (1.5 nmol, 6-24 MBq, final molar concentrations of 6.7-7.2 µM) and 2 µL of freshly prepared $ZnCl_2$ (1 mM). After shaking for 5 min, 5-25 µL neprilysin (Sigma-Aldrich, product no. SRP6450, stock of 50 µg/mL in PBS, final concentrations of 15-69 nM based in a molar mass of 80 kDa) was added. The mixture (final volumes of 207-227 µL) was incubated in a ThermoMixer Comfort 5355 (Eppendorf) at 37°C for up to 24 hours. At distinct time points aliquots of 25 µL were withdrawn and diluted with a minimum of 50 µL of a mixture named “Supersol”, which consists of 20% CH_3OH, 0.5% Triton X-100, 5 mM EDTA, 0.5 mM *o*-phenanthroline and 0.1% saponin. This was followed by centrifugation at 13,500 rpm for 3 min (Thermo Scientific Heraeus Fresco 21). The supernatant was analyzed by radio-HPLC. The equivalence of enzyme activity was secured by incubation of a reference compound on the same day.

Plasma stability assay

For human plasma, venous blood (4.5 mL) from one of two healthy, male volunteers who were not fasting or on any medication was collected. Blood samples were dispensed into S-Monovette® (Sarstedt) plasma separator tubes containing lithium heparin coated particles. The tubes were allowed to stand on ice for 30 min protected from light followed by centrifugation at 2000 rcf for 10 min at 4°C. Samples were visually checked for hemolysis and interference, stored at 4°C (protected from light) and used within 48 hours.

For pooled mouse plasma, arterial blood (>1 mL) from 3 mice was obtained by cardiac puncture. Blood samples were dispensed into lithium heparin (Heparin-Sodium LEO 25.000 I.U./5ml) flushed 1.5 ml Eppendorf tubes. The tubes were allowed to stand on ice for 30 min protected from light followed by centrifugation at 2000 rcf for 10 min at 4°C. Samples were visually checked for hemolysis and interference and lyophilized. On each day of testing the

solid was weight out and reconstituted with 9 parts MilliQ water (m/m). The equivalence of plasma sample activity was secured by incubation of a reference compound on the same day.

Alternatively, lyophilized, pooled mouse plasma containing 0.8% sodium citrate was purchased from Sigma-Aldrich (Product number P9275). On each day of testing the solid was weight out and reconstituted with 9 parts MilliQ water (w/w). The equivalence of plasma sample activity was secured by incubation of a reference compound on the same day.

For assessing the stability in plasma, 20 µL of the respective radiolabeled peptide (1 nmol, 19 MBq) were added to 280 µL plasma and the mixture was incubated in a ThermoMixer Comfort 5355 (Eppendorf) at 37°C for up to 24 hours. For assessing the stability in the presence of protease inhibitors, plasma was incubated with 10 µM phosphoramidon (stock of 1 mM in water) or 10 µM captopril (stock of 1 mM in water) for 10 min at 37°C prior to the addition of the radiolabeled peptide. At distinct time points an aliquot of 25 µL was withdrawn and diluted with a minimum of 50 µL of "Supersol". This was followed by centrifugation at 13,500 rpm for 3 min (Thermo Scientific Heraeus Fresco 21). The supernatant was analyzed by radio HPLC.

In vitro SST_2 binding affinity using live MPC cells

Mouse pheochromocytoma (MPC) cells (passages 35-40) were routinely cultured in collagen-coated flasks as described elsewhere.[45] A number of 3×10^5 cells/cm^2 were seeded in collagen-coated 48-well microplates and grown for three days. For binding assays, cell culture medium was removed and replaced by fresh medium supplemented with radioligand (A_m = 25 MBq/nmol) at increasing final concentrations between 0.321 and 40 nM (final sample volume 0.2 mL). Non-specific cell binding was measured in presence of non-labeled DOTA-TATE at a final concentration of 1 µM. Background binding to plastic surfaces was determined in cell-free wells. Samples were incubated for 60 min at 37°C. Incubation was stopped by washing with ice-cold Dulbecco's PBS. Cells were lysed with 0.1 M NaOH containing 1% (w/v) SDS. Activity was measured in cell lysates and in a series of radioligand standards containing increasing molar amounts between 0.06 and 8 pmol using the gamma counter Wizard (PerkinElmer). Protein content of cell lysates was measured at $A_{280\,nm}$ (setting 1 Abs = 1 mg/mL) using a nanodrop spectrophotometer (Thermo-Fisher Scientific). All measurements were performed in triplicates. Dissociation constants (K_d) and maximum binding capacities (B_{max}) were calculated as described in Figure S3 in Supporting Information.

Experimental animals[47]

Animal experiments were carried out according to the guidelines of the German Regulations for Animal Welfare and have been approved by the local Ethical Committee for Animal Experiments. A number of 4×10^6 MPC cells were re-suspended in 40 µL of Dulbecco's phosphate-buffered saline and injected subcutaneously into the shoulder of 7−10 week-old female nude mice (Rj:NMRI-Foxn1$^{nu/nu}$, Janvier Labs, Le Genest-Saint-Isle, France). General anesthesia was induced and maintained with inhalation of 10% (v/v) desflurane in 30/10% (v/v) oxygen/air. Tumor growth was monitored three times per week using caliper measurements. Animals were sacrificed using CO_2 inhalation and cervical dislocation.

Small animal PET/CT imaging

When diameters of MPC tumors reached 8 ± 3 mm, small-animal positron emission tomography (PET) was performed using the nanoScan® PET/CT (Mediso Medical Imaging Systems, Budapest, Hungary) and a Si78 PET/CT (BRUKER, Billerica, MA, USA). Scanners were cross-calibrated using a syringe source containing 10 MBq of [^{64}Cu]$CuCl_2$ diluted in 2 mL of 0.01 M HCl. Each mouse (n = 2) received between 7 and 10 MBq of the respective radioligand (A_m = 40 GBq/µmoL) delivered in 0.154 M NaCl via intravenous injection through a tail vein catheter within the initial 30 s after scan start. A series of PET/CT scans were performed at defined time points after radioligand injection (0-2 h [dynamically], 5 h [4.5-5.5 h], 20 h [19-21 h], 24 h [23-25 h], 40 h [39-41 h]). Image recording, image reconstruction and data analysis were performed as reported previously.[47] Standardized uptake values (SUV = [MBq detected activity/mL tissue] / [MBq injected activity/g body weight], mL/g) were determined in defined volumes of interest (VOIs) and reported as VOI-averaged SUVmean ± range [min–max].

Ex vivo metabolite analysis

For assessing the *in vivo* stability, **[^{64}Cu]Cu-NODAGA-NES4-TATE** or **[^{64}Cu]Cu-NODAGA-NES5-TATE** were injected *i.v.* into five healthy mice (injected activity of 26±1.3 MBq for NES4 and 25.2±0.4 MBq for NES5) under desflurane anesthesia (12% desflurane in 20% oxygen/air). At distinct time points (5, 15, 30, 60 and 120 min), the mice were sacrificed. Blood was obtained by cardiac puncture and was dispensed into lithium heparin (Heparin-Sodium LEO 25.000 I.U./5ml) flushed 1.5 ml Eppendorf tubes. This was followed by centrifugation at 13,000 g for 3 min. For protein precipitation, an aliquot (25 µL) of the resulting supernatant (plasma) was withdrawn and diluted with a minimum of 50 µL of "Supersol". The same

procedure was performed for a urine aliquot, which was obtained by puncture of the excised bladder. The “Supersol” mixtures were centrifuged at 13,500 rpm for 3 min. The supernatant was analyzed by radio HPLC. Kidney and liver were excised. Each organ was transferred into a 10 mL Vial and PBS (1 mL) was added. Homogenization was performed at 8,700 rpm (T25 ULTRA-TURRAX) for 3 min on ice. The resulting mixture was transferred into a 2 mL Vial and centrifuged (13,500 rpm for 3 min, Thermo Scientific Heraeus Fresco 21). Further processing of the supernatant was conducted as described for plasma and urine aliquots.

Associated Content

Supporting Information

Additional Discussions, Figures, Tables and Schemes (as mentioned in the text) and analytical data of the compounds (HPLC, HRMS)

Molecular formular strings

Author Information

*E-mail: r.wodtke@hzdr.de

Conflict of interest

There are no conflicts to declare.

Acknowledgments

This research was funded by Deutsche Forschungsgemeinschaft (DFG) within the Collaborative Research Center Transregio 205/1 and 205/2 “The Adrenal: Central Relay in Health and Disease” (CRC/TRR 205/1 and 205/2; M.U. and J.P.). We cordially appreciate the expert support of Andrea Suhr for performing ^{64}Cu-labeling and the various radiometric assay methods. We furthermore cordially acknowledge the participation of Dr. Markus Laube in fruitful discussions and for obtaining HR-MS spectra. The authors thank Dr. Martin Kreller and the cyclotron team as well as Dr. Martin Walther and Christian Jentschel for providing [^{64}Cu]$CuCl_2$. The excellent technical assistance of Mareike Barth regarding cell culture is greatly acknowledged. The authors thank the head and staff of the animal research facility, Dr. Birgit Belter, Katrin Baumgart, and Helge Gläser. Furthermore, the authors wish to thank Dr. Bianca Duss and Andrea Leuschner from BAD Gesundheitsvorsorge und Sicherheitstechnik

GmbH for blood draw. MPC 4/30PRR cells were kindly provided by Arthur Tischler, James Powers, and Karel Pacak.

Abbreviations used

ACE, angiotensin-converting enzyme; AUC, area under curve; BBMV…brush border membrane vesicle; NEP, neprilysin; NES, neprilysin substrate; PET, positron emission tomography; SST_2, somatostatin receptor subtype 2; SUV, standard uptake value.

References and Notes

1. Fendler, W. P.; Rahbar, K.; Herrmann, K.; Kratochwil, C. and Eiber, M. ^{177}Lu-PSMA radioligand therapy for prostate cancer. *J. Nucl. Med.*, **2017**, *58*, 1196-1200.
2. Hennrich, U. and Kopka, K. Lutathera®: the first FDA- and EMA-approved radiopharmaceutical for peptide receptor radionuclide therapy. *Pharmaceuticals*, **2019**, *12*.
3. Feijtel, D.; de Jong, M. and Nonnekens, J. Peptide receptor radionuclide therapy: looking back, looking forward. *Curr. Top. Med. Chem.*, **2020**, *20*, 2959-2969.
4. Strosberg, J.; El-Haddad, G.; Wolin, E.; Hendifar, A.; Yao, J.; Chasen, B.; Mittra, E.; Kunz, P. L.; Kulke, M. H.; Jacene, H.; Bushnell, D.; O'Dorisio, T. M.; Baum, R. P.; Kulkarni, H. R.; Caplin, M.; Lebtahi, R.; Hobday, T.; Delpassand, E.; Van Cutsem, E.; Benson, A.; Srirajaskanthan, R.; Pavel, M.; Mora, J.; Berlin, J.; Grande, E.; Reed, N.; Seregni, E.; Oberg, K.; Lopera Sierra, M.; Santoro, P.; Thevenet, T.; Erion, J. L.; Ruszniewski, P.; Kwekkeboom, D.; Krenning, E. and Investigators, N.-T. Phase 3 trial of ^{177}Lu-DOTATATE for midgut neuroendocrine tumors. *N. Engl. J. Med.*, **2017**, *376*, 125-135.
5. Sartor, O.; de Bono, J.; Chi, K. N.; Fizazi, K.; Herrmann, K.; Rahbar, K.; Tagawa, S. T.; Nordquist, L. T.; Vaishampayan, N.; El-Haddad, G.; Park, C. H.; Beer, T. M.; Armour, A.; Perez-Contreras, W. J.; DeSilvio, M.; Kpamegan, E.; Gericke, G.; Messmann, R. A.; Morris, M. J.; Krause, B. J. and Investigators, V. Lutetium-177-PSMA-617 for metastatic castration-resistant prostate cancer. *N. Engl. J. Med.*, **2021**, *385*, 1091-1103.
6. Haberkorn, U.; Mier, W.; Kopka, K.; Herold-Mende, C.; Altmann, A. and Babich, J. Identification of ligands and translation to clinical applications. *J. Nucl. Med.*, **2017**, *58*, 27S-33S.
7. Nicolas, G. P.; Morgenstern, A.; Schottelius, M. and Fani, M. New developments in peptide receptor radionuclide therapy. *J. Nucl. Med.*, **2019**, *60*, 167-171.
8. Reubi, J. C. and Maecke, H. R. Peptide-based probes for cancer imaging. *J. Nucl. Med.*, **2008**, *49*, 1735-1738.
9. Lee, S.; Xie, J. and Chen, X. Peptide-based probes for targeted molecular imaging. *Biochemistry*, **2010**, *49*, 1364-1376.
10. Vegt, E.; de Jong, M.; Wetzels, J. F.; Masereeuw, R.; Melis, M.; Oyen, W. J.; Gotthardt, M. and Boerman, O. C. Renal toxicity of radiolabeled peptides and antibody fragments: mechanisms, impact on radionuclide therapy, and strategies for prevention. *J. Nucl. Med.*, **2010**, *51*, 1049-1058.
11. Geenen, L.; Nonnekens, J.; Konijnenberg, M.; Baatout, S.; De Jong, M. and Aerts, A. Overcoming nephrotoxicity in peptide receptor radionuclide therapy using [^{177}Lu]Lu-DOTA-TATE for the treatment of neuroendocrine tumours. *Nucl. Med. Biol.*, **2021**, *102-103*, 1-11.
12. de Jong, M.; Barone, R.; Krenning, E.; Bernard, B.; Melis, M.; Visser, T.; Gekle, M.; Willnow, T. E.; Walrand, S.; Jamar, F. and Pauwels, S. Megalin is essential for renal proximal tubule reabsorption of ^{111}In-DTPA-Octreotide. *J. Nucl. Med.*, **2005**, *46*, 1696-1700.
13. Melis, M.; Krenning, E. P.; Bernard, B. F.; Barone, R.; Visser, T. J. and de Jong, M. Localisation and mechanism of renal retention of radiolabelled somatostatin analogues. *Eur. J. Nucl. Med. Mol. Imaging*, **2005**, *32*, 1136-1143.
14. Christensen, E. I.; Birn, H.; Verroust, P. and Moestrup, S. K. Megalin-mediated endocytosis in renal proximal tubule. *Ren. Fail.*, **1998**, *20*, 191-199.
15. Christensen, E. I.; Birn, H.; Storm, T.; Weyer, K. and Nielsen, R. Endocytic receptors in the renal proximal tubule. *Physiology*, **2012**, *27*, 223-236.
16. Nielsen, R.; Christensen, E. I. and Birn, H. Megalin and cubilin in proximal tubule protein reabsorption: from experimental models to human disease. *Kidney Int.*, **2016**, *89*, 58-67.
17. Vegt, E.; Melis, M.; Eek, A.; de Visser, M.; Brom, M.; Oyen, W. J.; Gotthardt, M.; de Jong, M. and Boerman, O. C. Renal uptake of different radiolabelled peptides is mediated by megalin: SPECT and biodistribution studies in megalin-deficient mice. *Eur. J. Nucl. Med. Mol. Imaging*, **2011**, *38*, 623-632.

18. Bass, L. A.; Lanahan, M. V.; Duncan, J. R.; Erion, J. L.; Srinivasan, A.; Schmidt, M. A. and Anderson, C. J. Identification of the soluble in vivo metabolites of indium-111-diethylenetriaminepentaacetic acid-D-Phe^{1}-octreotide. *Bioconjug. Chem.*, **1998**, *9*, 192-200.
19. Akizawa, H.; Arano, Y.; Uezono, T.; Ono, M.; Fujioka, Y.; Uehara, T.; Yokoyama, A.; Akaji, K.; Kiso, Y.; Koizumi, M. and Saji, H. Renal metabolism of ^{111}In-DTPA-D-Phe^{1}-octreotide in vivo. *Bioconjug. Chem.*, **1998**, *9*, 662-670.
20. Chigoho, D. M.; Bridoux, J. and Hernot, S. Reducing the renal retention of low- to moderate-molecular-weight radiopharmaceuticals. *Curr. Opin. Chem. Biol.*, **2021**, *63*, 219-228.
21. Rolleman, E. J.; Melis, M.; Valkema, R.; Boerman, O. C.; Krenning, E. P. and de Jong, M. Kidney protection during peptide receptor radionuclide therapy with somatostatin analogues. *Eur. J. Nucl. Med. Mol. Imaging*, **2010**, *37*, 1018-1031.
22. FDA drug label, https://www.accessdata.fda.gov/drugsatfda_docs/nda/2018/208700Orig1s000lbll.pdf, (accessed 19/08/22).
23. Mogensen, C. E. and Solling Studies on renal tubular protein reabsorption: partial and near complete inhibition by certain amino acids. *Scand. J. Clin. Lab. Invest.*, **1977**, *37*, 477-486.
24. Gotthardt, M.; van Eerd-Vismale, J.; Oyen, W. J.; de Jong, M.; Zhang, H.; Rolleman, E.; Maecke, H. R.; Behe, M. and Boerman, O. Indication for different mechanisms of kidney uptake of radiolabeled peptides. *J. Nucl. Med.*, **2007**, *48*, 596-601.
25. Arano, Y. Renal brush border strategy: A developing procedure to reduce renal radioactivity levels of radiolabeled polypeptides. *Nucl. Med. Biol.*, **2021**, *92*, 149-155.
26. Lau, J.; Lee, H.; Rousseau, J.; Benard, F. and Lin, K. S. Application of cleavable linkers to improve therapeutic index of radioligand therapies. *Molecules*, **2022**, *27*, 4959.
27. Arano, Y.; Fujioka, Y.; Akizawa, H.; Ono, M.; Uehara, T.; Wakisaka, K.; Nakayama, M.; Sakahara, H.; Konishi, J. and Saji, H. Chemical design of radiolabeled antibody fragments for low renal radioactivity levels. *Cancer Res.*, **1999**, *59*, 128-134.
28. Fujioka, Y.; Satake, S.; Uehara, T.; Mukai, T.; Akizawa, H.; Ogawa, K.; Saji, H.; Endo, K. and Arano, Y. In vitro system to estimate renal brush border enzyme-mediated cleavage of peptide linkages for designing radiolabeled antibody fragments of low renal radioactivity levels. *Bioconjug. Chem.*, **2005**, *16*, 1610-1616.
29. Uehara, T.; Koike, M.; Nakata, H.; Hanaoka, H.; Iida, Y.; Hashimoto, K.; Akizawa, H.; Endo, K. and Arano, Y. Design, synthesis, and evaluation of [^{188}Re]organorhenium-labeled antibody fragments with renal enzyme-cleavable linkage for low renal radioactivity levels. *Bioconjug. Chem.*, **2007**, *18*, 190-198.
30. Uehara, T.; Yokoyama, M.; Suzuki, H.; Hanaoka, H. and Arano, Y. A gallium-67/68-labeled antibody fragment for immuno-SPECT/PET shows low renal radioactivity without loss of tumor uptake. *Clin. Cancer Res.*, **2018**, *24*, 3309-3316.
31. Suzuki, C.; Uehara, T.; Kanazawa, N.; Wada, S.; Suzuki, H. and Arano, Y. Preferential cleavage of a tripeptide linkage by enzymes on renal brush border membrane to reduce renal radioactivity levels of radiolabeled antibody fragments. *J. Med. Chem.*, **2018**, *61*, 5257-5268.
32. Hooper, N. M. Families of zinc metalloproteases. *FEBS Lett.*, **1994**, *354*, 1-6.
33. Turner, A. J. and Nalivaeva, N. N., Chapter 241 - Peptide Degradation (Neprilysin and Other Regulatory Peptidases). In *Handbook of biologically active peptides (Second Edition)*, Ed. A. J. Kastin, Academic Press, 2013, pp. 1757-1764.
34. Bayes-Genis, A.; Barallat, J. and Richards, A. M. A test in context: neprilysin: function, inhibition, and biomarker. *J. Am. Coll. Cardiol.*, **2016**, *68*, 639-653.
35. Feygina, E. E.; Katrukha, A. G. and Semenov, A. G. Neutral endopeptidase (neprilysin) in therapy and diagnostics: yin and yang. *Biochemistry*, **2019**, *84*, 1346-1358.
36. Nalivaeva, N. N. and Turner, A. J., Chapter 127 - Neprilysin. In *Handbook of Proteolytic Enzymes*, Eds. N. D. Rawlings and G. Salvesen, Academic Press, 2013, DOI: 10.1016/b978-0-12-382219-2.00127-7, pp. 612-619.
37. George, S. G. and Kenny, J. Studies on the enzymology of purified preparations of brush border from rabbit kidney. *Biochem. J.*, **1973**, *134*, 43-57.
38. Kerr, M. A. and Kenny, A. J. The purification and specificity of a neutral endopeptidase from rabbit kidney brush border. *Biochem. J.*, **1974**, *137*, 477-488.
39. Zhang, M.; Ye, J.; Xie, Z.; Yan, Y.; Wang, J. and Chen, X. Optimization of enzymolysis clearance strategy to enhance renal clearance of radioligands. *Bioconjug. Chem.*, **2021**, *32*, 2108-2116.
40. Zhang, M.; Ye, J.; Xie, Z.; Wang, Y.; Ma, W.; Kang, F.; Yang, W.; Wang, J. and Chen, X. Combined probe strategy to increase the enzymatic digestion rate and accelerate the renal radioactivity clearance of peptide radiotracers. *Mol. Pharm.*, **2022**, *19*, 1548-1556.
41. Yim, C. B.; Mikkola, K.; Fagerholm, V.; Elomaa, V. V.; Ishizu, T.; Rajander, J.; Schlesinger, J.; Roivainen, A.; Nuutila, P. and Solin, O. Synthesis and preclinical characterization of [^{64}Cu]NODAGA-MAL-exendin-4 with a N^{ε}-maleoyl-L-lysyl-glycine linkage. *Nucl. Med. Biol.*, **2013**, *40*, 1006-1012.
42. Zhang, M.; Jacobson, O.; Kiesewetter, D. O.; Ma, Y.; Wang, Z.; Lang, L.; Tang, L.; Kang, F.; Deng, H.; Yang, W.; Niu, G.; Wang, J. and Chen, X. Improving the theranostic potential of exendin 4 by reducing the renal radioactivity through brush border membrane enzyme-mediated degradation. *Bioconjug. Chem.*, **2019**, *30*, 1745-1753.

43. Vaidyanathan, G.; Kang, C. M.; McDougald, D.; Minn, I.; Brummet, M.; Pomper, M. G. and Zalutsky, M. R. Brush border enzyme-cleavable linkers: Evaluation for reducing renal uptake of radiolabeled prostate-specific membrane antigen inhibitors. *Nucl. Med. Biol.*, **2018**, *62-63*, 18-30.
44. Bendre, S.; Zhang, Z.; Kuo, H. T.; Rousseau, J.; Zhang, C.; Merkens, H.; Roxin, A.; Benard, F. and Lin, K. S. Evaluation of Met-Val-Lys as a renal brush border enzyme-cleavable linker to reduce kidney uptake of ^{68}Ga-labeled DOTA-conjugated peptides and peptidomimetics. *Molecules*, **2020**, *25*, 3854.
45. Ullrich, M.; Bergmann, R.; Peitzsch, M.; Cartellieri, M.; Qin, N.; Ehrhart-Bornstein, M.; Block, N. L.; Schally, A. V.; Pietzsch, J.; Eisenhofer, G.; Bornstein, S. R. and Ziegler, C. G. In vivo fluorescence imaging and urinary monoamines as surrogate biomarkers of disease progression in a mouse model of pheochromocytoma. *Endocrinology*, **2014**, *155*, 4149-4156.
46. Ullrich, M.; Bergmann, R.; Peitzsch, M.; Zenker, E. F.; Cartellieri, M.; Bachmann, M.; Ehrhart-Bornstein, M.; Block, N. L.; Schally, A. V.; Eisenhofer, G.; Bornstein, S. R.; Pietzsch, J. and Ziegler, C. G. Multimodal somatostatin receptor theranostics using [^{64}Cu]Cu-/[^{177}Lu]Lu-DOTA-(Tyr^{3})octreotate and AN-238 in a mouse pheochromocytoma model. *Theranostics*, **2016**, *6*, 650-665.
47. Brandt, F.; Ullrich, M.; Laube, M.; Kopka, K.; Bachmann, M.; Löser, R.; Pietzsch, J.; Pietzsch, H. J.; van den Hoff, J. and Wodtke, R. "Clickable" albumin binders for modulating the tumor uptake of targeted radiopharmaceuticals. *J. Med. Chem.*, **2022**, *65*, 710-733.
48. Schechter, I. and Berger, A. On the size of the active site in proteases. I. Papain. *Biochem Bioph Res Co*, **2012**, *425*, 497-502.
49. Mital, M.; Bal, W.; Fraczyk, T. and Drew, S. C. Interplay between copper, neprilysin, and N-truncation of beta-amyloid. *Inorg. Chem.*, **2018**, *57*, 6193-6197.
50. Barros, N. M.; Campos, M.; Bersanetti, P. A.; Oliveira, V.; Juliano, M. A.; Boileau, G.; Juliano, L. and Carmona, A. K. Neprilysin carboxydipeptidase specificity studies and improvement in its detection with fluorescence energy transfer peptides. *Biol. Chem.*, **2007**, *388*, 447-455.
51. Rostkowska, H.; Lapinski, L.; Khvorostov, A. and Nowak, M. J. Proton-transfer processes in thiourea: UV induced thione → thiol reaction and ground state thiol → thione tunneling. *J. Phys. Chem. A*, **2003**, *107*, 6373-6380.
52. Kalichkina, L. E.; Bakibaev, A. A. and Malkov, V. S. Spectral study of thione-thiol tautomerization of thiourea in aqueous alcohol solution. *Bulletin of the Karaganda University.*, **2020**, *99*, 66-71.
53. Edman, P. Method for determination of the amino acid sequence in peptides. *Acta Chem. Scand.*, **1950**, *4*, 283-293.
54. Edman, P. On the mechanism of the phenyl isothiocyanate degradation of peptides. *Acta Chem. Scand.*, **1956**, *10*, 761-768.
55. Lang, L.; Ma, Y.; Kiesewetter, D. O. and Chen, X. Stability analysis of glutamic acid linked peptides coupled to NOTA through different chemical linkages. *Mol. Pharm.*, **2014**, *11*, 3867-3874.
56. Schlesinger, J.; Rajander, J.; Ihalainen, J. A.; Ramesh, D.; Eklund, P.; Fagerholm, V.; Nuutila, P. and Solin, O. Isomerism of [^{64}Cu-NOTA-Bn]-labeled radiotracers: separation of two complex isomers and determination of their interconversion energy barrier using ion pair chromatography. *Inorg. Chem.*, **2011**, *50*, 4260-4271.
57. Gao, F.; Sihver, W.; Bergmann, R.; Walther, M.; Stephan, H.; Belter, B.; Neuber, C.; Haase-Kohn, C.; Bolzati, C.; Pietzsch, J. and Pietzsch, H. J. Radiochemical and radiopharmacological characterization of a (64) Cu-labeled alpha-MSH analog conjugated with different chelators. *J. Labelled Comp. Radiopharm.*, **2019**, *62*, 495-509.
58. Grob, N. M.; Behe, M.; von Guggenberg, E.; Schibli, R. and Mindt, T. L. Methoxinine - an alternative stable amino acid substitute for oxidation-sensitive methionine in radiolabelled peptide conjugates. *J. Pept. Sci.*, **2017**, *23*, 38-44.
59. Suzuki, H.; Kise, S.; Kaizuka, Y.; Watanabe, R.; Sugawa, T.; Furukawa, T.; Fujii, H. and Uehara, T. Copper-64-labeled antibody fragments for immuno-PET/radioimmunotherapy with low renal radioactivity levels and amplified tumor-kidney ratios. *ACS Omega*, **2021**, *6*, 21556-21562.
60. Medeiros, M. A. S.; Franca, M. S. F.; Boileau, G.; Juliano, L. and Carvalho, K. M. Specific fluorogenic substrates for neprilysin (neutral endopeptidase, EC 3.4.24.11) which are highly resistant to serine- and metalloproteases. *Braz. J. Med. Biol. Res.*, **1997**, *30*, 1157-1162.
61. Jeng, A. Y.; Ansell, J. and Erion, M. D. pH- and time-dependent inhibition of rat kidney neutral endoprotease 24.11 by thiorphan and phosphoramidon. *Life Sci.*, **1989**, *45*, 2109-2114.
62. Oh, H.; Kang, D. G.; Kwon, J. W.; Kwon, T. O.; Lee, S. Y.; Lee, D. B. and Lee, H. S. Isolation of angiotensin converting enzyme (ACE) inhibitory flavonoids from *Sedum sarmentosum*. *Biol. Pharm. Bull.*, **2004**, *27*, 2035-2037.
63. Campbell, D. J. Neprilysin Inhibitors and Bradykinin. *Front. Med .* **2018**, *5*, 257.
64. Kukkola, P. J.; Savage, P.; Sakane, Y.; Berry, J. C.; Bilci, N. A.; Ghai, R. D. and Jeng, A. Y. Differential structure-activity relationships of phosphoramidon analogues for inhibition of three metalloproteases: endothelin-converting enzyme, neutral endopeptidase, and angiotensin-converting enzyme. *J. Cardiovasc. Pharmacol.*, **1995**, *26 Suppl 3*, S65-68.
65. Graf, K.; Koehne, P.; Grafe, M.; Zhang, M.; Auch-Schwelk, W. and Fleck, E. Regulation and differential expression of neutral endopeptidase 24.11 in human endothelial cells. *Hypertension*, **1995**, *26*, 230-235.
66. Fitzpatrick, P. A.; Guinan, A. F.; Walsh, T. G.; Murphy, R. P.; Killeen, M. T.; Tobin, N. P.; Pierotti, A. R. and Cummins, P. M. Down-regulation of neprilysin (EC3.4.24.11) expression in vascular endothelial cells by

laminar shear stress involves NADPH oxidase-dependent ROS production. *Int. J. Biochem. Cell Biol.*, **2009**, *41*, 2287-2294.
67. Nock, B. A.; Maina, T.; Krenning, E. P. and de Jong, M. "To serve and protect": enzyme inhibitors as radiopeptide escorts promote tumor targeting. *J. Nucl. Med.*, **2014**, *55*, 121-127.
68. Kaloudi, A.; Nock, B. A.; Lymperis, E.; Valkema, R.; Krenning, E. P.; de Jong, M. and Maina, T. Impact of clinically tested NEP/ACE inhibitors on tumor uptake of [^{111}In-DOTA]MG11-first estimates for clinical translation. *EJNMMI Res.*, **2016**, *6*, 15.
69. Kaloudi, A.; Nock, B. A.; Lymperis, E.; Krenning, E. P.; de Jong, M. and Maina, T. ^{99m}Tc-labeled gastrins of varying peptide chain length: Distinct impact of NEP/ACE-inhibition on stability and tumor uptake in mice. *Nucl. Med. Biol.*, **2016**, *43*, 347-354.
70. Kaloudi, A.; Nock, B. A.; Lymperis, E.; Krenning, E. P.; de Jong, M. and Maina, T. Improving the In vivo profile of minigastrin radiotracers: a comparative study involving the neutral endopeptidase inhibitor phosphoramidon. *Cancer Biother. Radiopharm.*, **2016**, *31*, 20-28.
71. Ahn, K.; Herman, S. B. and Fahnoe, D. C. Soluble human endothelin-converting enzyme-1: expression, purification, and demonstration of pronounced pH sensitivity. *Arch. Biochem. Biophys.*, **1998**, *359*, 258-268.
72. Ohnaka, K.; Takayanagi, R.; Nishikawa, M.; Haji, M. and Nawata, H. Purification and characterization of a phosphoramidon-sensitive endothelin-converting enzyme in porcine aortic endothelium. *J. Biol. Chem.*, **1993**, *268*, 26759-26766.
73. Whyteside, A. R. and Turner, A. J., Chapter 129 - Endothelin-converting enzyme-1 (ECE-1). In *Handbook of Proteolytic Enzymes*, Eds. N. D. Rawlings and G. Salvesen, Academic Press, 2013, pp. 624-631.
74. Khamaisi, M.; Toukan, H.; Axelrod, J. H.; Rosenberger, C.; Skarzinski, G.; Shina, A.; Meidan, R.; Koesters, R.; Rosen, S.; Walkinshaw, G.; Mimura, I.; Nangaku, M. and Heyman, S. N. Endothelin-converting enzyme is a plausible target gene for hypoxia-inducible factor. *Kidney Int.*, **2015**, *87*, 761-770.
75. Kumar, R.; Adiga, A.; Novack, J.; Etinger, A.; Chinitz, L.; Slater, J.; de Loor, H.; Meijers, B.; Holzman, R. S. and Lowenstein, J. The renal transport of hippurate and protein-bound solutes. *Physiol. Rep.*, **2020**, *8*, e14349.
76. Kuo, H. T.; Pan, J.; Zhang, Z.; Lau, J.; Merkens, H.; Zhang, C.; Colpo, N.; Lin, K. S. and Benard, F. Effects of linker modification on tumor-to-kidney contrast of ^{68}Ga-labeled PSMA-targeted imaging probes. *Mol. Pharm.*, **2018**, *15*, 3502-3511.
77. Oefner, C.; D'Arcy, A.; Hennig, M.; Winkler, F. K. and Dale, G. E. Structure of human neutral endopeptidase (Neprilysin) complexed with phosphoramidon. *J. Mol. Biol.*, **2000**, *296*, 341-349.
78. Pankow, K.; Schwiebs, A.; Becker, M.; Siems, W. E.; Krause, G. and Walther, T. Structural substrate conditions required for neutral endopeptidase-mediated natriuretic peptide degradation. *J. Mol. Biol.*, **2009**, *393*, 496-503.
79. Uehara, T.; Kanazawa, N.; Suzuki, C.; Mizuno, Y.; Suzuki, H.; Hanaoka, H. and Arano, Y. Renal handling of ^{99m}Tc-labeled antibody Fab fragments with a linkage cleavable by enzymes on brush border membrane. *Bioconjug. Chem.*, **2020**, *31*, 2618-2627.
80. Tojo, A. and Endou, H. Intrarenal handling of proteins in rats using fractional micropuncture technique. *Am. J. Physiol.*, **1992**, *263*, F601-606.
81. Gekle, M. Renal proximal tubular albumin reabsorption: daily prevention of albuminuria. *News Physiol. Sci.*, **1998**, *13*, 5-11.
82. Tojo, A. The role of the kidney in protein metabolism: the capacity of tubular lysosomal proteolysis in nephrotic syndrome. *Kidney Int.*, **2013**, *84*, 861-863.
83. Heneweer, C.; Holland, J. P.; Divilov, V.; Carlin, S. and Lewis, J. S. Magnitude of enhanced permeability and retention effect in tumors with different phenotypes: ^{89}Zr-albumin as a model system. *J. Nucl. Med.*, **2011**, *52*, 625-633.
84. Jodal, A.; Pape, F.; Becker-Pauly, C.; Maas, O.; Schibli, R. and Behe, M. Evaluation of ^{111}In-labelled exendin-4 derivatives containing different meprin beta-specific cleavable linkers. *PLoS One*, **2015**, *10*, e0123443.
85. Erdös, E. G. and Skidgel, R. A. Neutral endopeptidase 24.11 (enkephalinase) and related regulators of peptide hormones. *FASEB J.*, **1989**, *3*, 145-151.
86. Kounnas, M. Z.; Wolz, R. L.; Gorbea, C. M. and Bond, J. S. Meprin-A and -B. Cell surface endopeptidases of the mouse kidney. *J. Biol. Chem.*, **1991**, *266*, 17350-17357.
87. Kaushal, G. P.; Haun, R. S.; Herzog, C. and Shah, S. V. Meprin A metalloproteinase and its role in acute kidney injury. *Am. J. Physiol. Renal Physiol.*, **2013**, *304*, F1150-1158.
88. Walmsley, S. J.; Broeckling, C.; Hess, A.; Prenni, J. and Curthoys, N. P. Proteomic analysis of brush-border membrane vesicles isolated from purified proximal convoluted tubules. *Am. J. Physiol. Renal Physiol.*, **2010**, *298*, F1323-1331.
89. Avdeev, D. V.; Ovchinnikov, M. V.; Dudkina, Y. S.; Molokoedov, A. S.; Azmuko, A. A.; Palkeeva, M. E. and Sidorova, M. V. Optimal Method for Disulfide Bond Closure in the Synthesis of Atosiban—Antagonist of Oxytocin Receptors. *Russ. J. Bioorganic Chem.*, **2021**, *47*, 1241-1248.
90. Thieme, S.; Walther, M.; Pietzsch, H. J.; Henniger, J.; Preusche, S.; Mading, P. and Steinbach, J. Module-assisted preparation of ^{64}Cu with high specific activity. *Appl. Radiat. Isot.*, **2012**, *70*, 602-608.
91. Kreller, M.; Pietzsch, H.; Walther, M.; Tietze, H.; Kaever, P.; Knieß, T.; Füchtner, F.; Steinbach, J. and Preusche, S. Introduction of the new center for radiopharmaceutical cancer research at Helmholtz-Zentrum Dresden-Rossendorf. *Instruments*, **2019**, *3*, 9.

Table of Content